

## 5. THE ARCTIC—M. O. Jeffries and J. Richter-Menge, Eds.

### a. Overview—M. O. Jeffries and J. Richter-Menge

The climate of the Arctic in 2012 was dominated by continued significant changes in the cryosphere. There were new records for minimum sea ice extent and permafrost warming in northernmost Alaska. And, a negative North Atlantic Oscillation (NAO) in spring and summer, which promoted southerly airflow into the Arctic, had a major impact on lake ice break-up, snow cover extent, Greenland Ice Sheet melt extent and albedo, and mass loss from the ice sheet and from Canadian Arctic glaciers and ice caps.

Lake ice break-up was up to three weeks earlier in Arctic Canada and up to one month earlier in Eurasia, consistent with changes in spring snow cover extent. A new record low Northern Hemisphere snow cover extent occurred in June, and June snow cover extent is now declining at a faster rate (-17.6% per decade) than September sea ice extent (-13.0% per decade).

The strong negative NAO caused persistent high sea level pressure over Greenland, a feature of the last six summers, and record air temperatures in June, July, and August (JJA). Consequently, new ice sheet surface melt and albedo records occurred. A rare 97% melt extent on 11–12 July was almost four times the mean melt extent during 1981–2010. The mass loss,  $-627 \pm 89$  Gt, from the Greenland Ice Sheet in JJA was a new record. The atmospheric circulation responsible for the extraordinary events in Greenland also affected Canadian Arctic glaciers and ice caps, where the mass loss for balance year 2011/12,  $-106 \pm 27$  Gt, equaled the record set the previous year.

Sea surface temperatures (SST) in Baffin Bay, between Greenland and the Canadian Arctic, were  $>2^{\circ}\text{C}$  higher in August than the mean August SST during 1982–2006. Similar August SST anomalies occurred in the Arctic Ocean. The exception was a negative SST anomaly in the Chukchi Sea, where locally extensive ice cover remained, even as the main body of the pack ice retreated northward and reached a new record minimum extent of  $3.41 \times 10^6$  km<sup>2</sup> in mid-September. An intense cyclone (ranked 13 out of 19 625 such storms that have occurred since 1979 in the Arctic) in early August contributed to the sea ice retreat.

A contrast in aragonite saturation state, a measure of ocean acidification, was observed between the Chukchi Sea and the Beaufort Sea/Canada Basin, where surface waters were almost undersaturated with respect to aragonite. The Beaufort Gyre, Canada Basin, continued to have the maximum freshwater content in the Arctic Ocean, the 2012 value being

similar to that of 2011. The heat content of the Beaufort Gyre in 2012 was also similar to 2011, both averaging ~25% more in summer compared to the 1970s.

At the southern boundary of the Beaufort Sea, on the North Slope of Alaska, new record high temperatures occurred at 20 m below the surface at most permafrost observatories. The record temperatures are part of a ~30-year warming trend that began near the coast in the 1970s and which now appears to be propagating inland. Throughout the Arctic, cold, coastal permafrost has been warming for several decades, while the temperature of warmer, inland permafrost has been relatively stable or even decreasing slightly.

Atmospheric CO<sub>2</sub> and CH<sub>4</sub> concentrations continue to rise, and the former exceeded 400 ppm at a number of Arctic sites for the first time. Notwithstanding the permafrost warming trends, there is no evidence that increasing Arctic atmospheric CH<sub>4</sub> concentrations are due to increasing emissions from Arctic sources.

Atmospheric total ozone columns were considerably higher than those in spring 2011, when unprecedented chemical ozone losses occurred. Ultraviolet radiation levels during the first half of 2012 were generally within the range observed during the last two decades.

### b. Air temperature, atmospheric circulation, and clouds—J. Overland, J. Key, B.-M. Kim, S.-J. Kim, Y. Liu, J. Walsh, M. Wang, U. Bhatt, and R. Thoman

#### 1) MEAN ANNUAL SURFACE AIR TEMPERATURE

In contrast to the period 2001–11, when large positive Arctic-wide temperature anomalies occurred, 2012 had relatively weak positive annual temperature anomalies in the central Arctic, with a small region of maximum positive temperature anomalies over the coast of subarctic central Siberia and adjacent waters (Fig. 5.1a). However, the Arctic continues to show local monthly extremes, with several Alaska stations reporting the coldest month on record in January, and Barrow, in northernmost Alaska, recording the warmest October in more than nine decades of unbroken climate observations. Record summer temperatures over Greenland (section 5g) were another regional/seasonal extreme.

On a decadal timescale, substantial positive temperature anomalies have been observed everywhere across the central Arctic during the period 2001–12 relative to a 1971–2000 reference period (Fig. 5.1b; Overland et al. 2011a; Stroeve et al. 2012, updated). This temperature pattern is a manifestation of "Arctic amplification", which is characterized by temperature

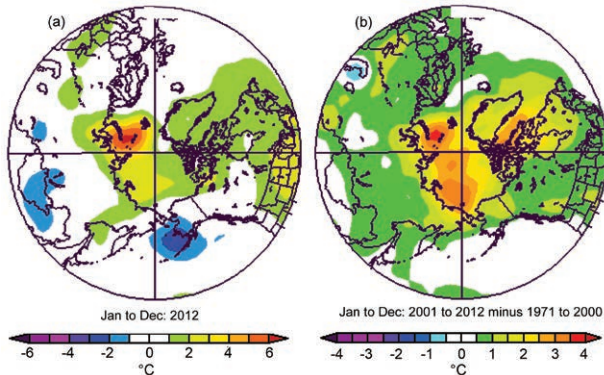


**FIG. 5.1. (a) Annual average near-surface air temperature anomalies for 2012 relative to the 1981–2010 reference period. (b) Annual average near-surface air temperature anomalies for the period 2001–12 relative to the reference period 1971–2000. (Source: NOAA/ESRL, <http://www.esrl.noaa.gov/psd/>.)**

increases 1.5°C greater than (more than double) the increases at lower latitudes. Since the mid-1960s, mean annual surface air temperature over Arctic land areas has increased about 2°C (Overland et al. 2012a).

## 2) SEASONAL AIR TEMPERATURES

Consistent with the annual average temperatures (Fig. 5.1), each seasonal near-surface air temperature anomaly distribution shows generally positive departures across the Arctic, with regional maxima often centered in the subarctic (Fig. 5.2). Winter 2012 was characterized by a positive North Atlantic Oscillation (NAO), which promotes the warm temperature anomaly over the Barents and Kara Seas (Fig. 5.2a) through warm air advection and increased storm activity downstream of the stronger winds and lower pressures of the Icelandic low pressure center. The temperature pattern in 2012 was unlike the Warm Arctic/Cold Continents pattern (e.g., Overland et al. 2010, 2011b) associated with a negative Arctic Oscillation (AO) climate pattern over the central Arctic, which dominated fall 2009 and 2010, and winter 2010 and 2011.

In contrast to the positive winter NAO, spring and summer had a negative NAO, with its more meridional (north-south, south-north) wind pattern. This had significant consequences for snow cover duration (section 5e), lake ice break-up (section 5i), and the extent of melting on the Greenland Ice Sheet (section 5g). Spring also saw the early formation of an Arctic dipole pattern, with high pressure on the North American side of the Arctic and low pressure on the Siberian side (Fig. 5.3a). In the previous five years this did not occur until June (Overland et al. 2012b). The Arctic dipole pattern supported increased

winds across the Arctic and warmer temperature anomalies over the East Siberian Sea and western Greenland (Fig. 5.2b). In contrast to previous years, and especially 2007, the Arctic dipole in 2012 was short-lived, with summer mostly characterized by low pressure centered on the Pacific Arctic sector (Figs. 5.2c and 5.3b), similar to climate conditions of the late 20th century. An unusually strong summer storm in early August (Sidebar 5.1) contributed to the summer low pressure average, with the exception of Greenland (Fig. 5.3b).

Despite the early deterioration of the Arctic dipole pattern, high sea level pressure persisted over Greenland (Fig. 5.3b). This has been a feature of early summer for the last six years. Higher pressures over Greenland and their influence on Arctic and subarctic wind patterns, a so-called blocking pattern, suggests physical connections between the wind patterns and reduced North American snow cover in May and June (section 5e), loss of Greenland and Canadian Arctic glacier ice (sections 5f and 5g), reduced Arctic sea ice in the summer (section 5j), and, potentially, extremes in mid-latitude weather (Overland et al. 2012b).

Fall was dominated by warm air anomalies lying primarily over regions that were sea ice free in late summer, i.e., the Barents, East Siberian, and Beau-

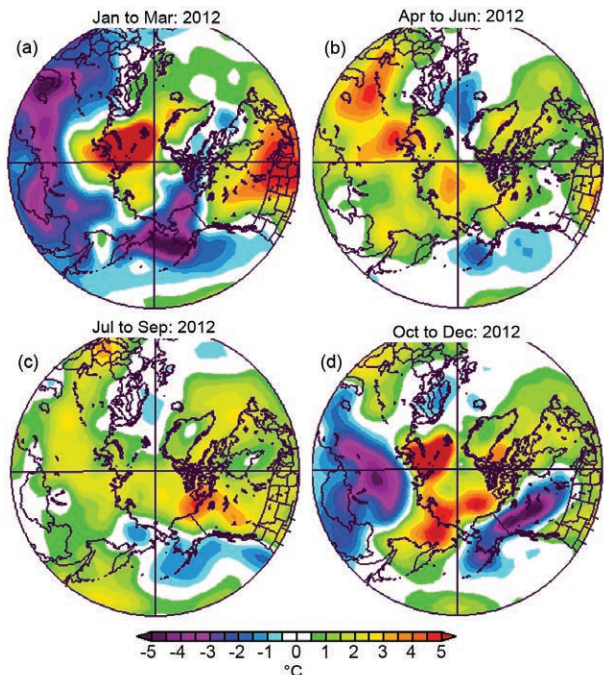


**FIG. 5.2. Seasonal anomaly patterns for near-surface air temperatures in 2012 relative to the reference period 1981–2010: winter (a), spring (b), summer (c), and fall (d). (Source: NOAA/ESRL, <http://www.esrl.noaa.gov/psd/>.)**

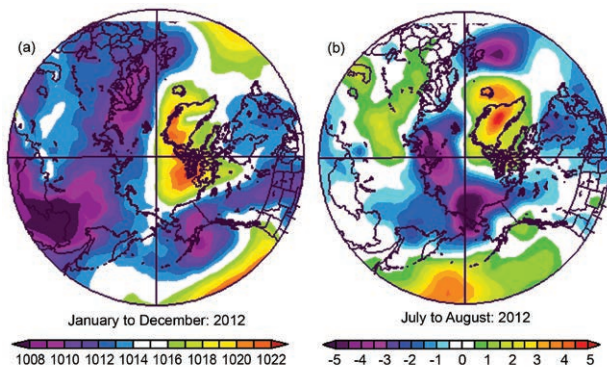


**FIG. 5.3. (a) Sea level pressure for Apr–Jun 2012 showing the Arctic dipole pattern, with high pressure on the North American side of the Arctic and low pressure on the Eurasian side. (b) Sea level pressure anomaly for Jul and Aug 2012 relative to the reference period 1981–2010, with extensive low pressure centered on the Pacific Arctic sector and high pressure over Greenland. (Source: NOAA/ESRL, <http://www.esrl.noaa.gov/psd/>.)**

fort Seas and northern Baffin Bay (Fig. 5.2d). The AO index was again negative in fall, similar to 2009 and 2010, favoring a more meridional wind pattern and potentially increased Arctic-subarctic weather linkages (Francis and Vavrus 2012; J. Liu et al. 2012). These linkages are a controversial topic and an area of active research.

### 3) SEVERE WEATHER

The year 2012 was notable for two severe weather events. One, an extreme cyclone in August in the Pacific Arctic sector, is described by Simmonds (Sidebar 5.1).

The other severe weather event was in late January–early February, when a warm center occurred over the Kara and Laptev Seas and broader, severe cold anomalies occurred over the northern Eurasian subarctic during a brief period of negative AO. There was a sharp contrast in surface temperature anomalies between North America and Eurasia. The United States experienced its fourth warmest winter since national records began in 1895, whereas extremely low temperatures occurred across parts of Eurasia during 24 January–14 February (see Sidebar 7.4). This was Europe's worst cold spell in at least 26 years, and more than 650 people died as a result of frigid conditions in Russia, Ukraine, and Poland. Snow fell across the affected areas, resulting in the third largest February snow cover extent (<http://www.ncdc.noaa.gov/sotc/global-snow/2012/2>).

### 4) CLOUD COVER

Unlike 2011, when Arctic cloud cover was somewhat higher than normal in winter and lower in the summer, Arctic cloud cover in 2012 was, overall, average compared to the period 2001–10. However, there were significant monthly anomalies that warrant closer examination, as the spatial patterns varied in important ways on the regional scale.

While clouds influence the surface energy budget, they also respond to changes in the ice cover (Y. Liu et al. 2012; Schweiger et al. 2008). As in recent years, positive cloud cover anomalies (more cloud) over the Arctic Ocean correspond to negative sea ice concentration anomalies (less ice). This was particularly evident in the winter months in the Barents and Kara Seas region, and in the summer months from the East Siberian Sea to the Beaufort Sea. An example for September 2012 is shown in Fig. 5.4.

Large-scale advection of heat and moisture and the frequency of synoptic scale systems also influence cloud cover (Liu et al. 2007). For example, positive cloud anomalies over Alaska in September correspond to southerly flow on the eastern side of the monthly mean cyclonic circulation pattern, while negative cloud anomalies over Russia during the same month correspond to northerly flow and the Siberian High. Positive cloud anomalies over the Chukchi Sea in June also appear to be related more to changes in circulation than to changes in sea ice cover. These circulation patterns are evident in the 500 hPa geopotential height and wind anomalies (not shown), and can be inferred from the surface temperature fields in Fig. 5.2.

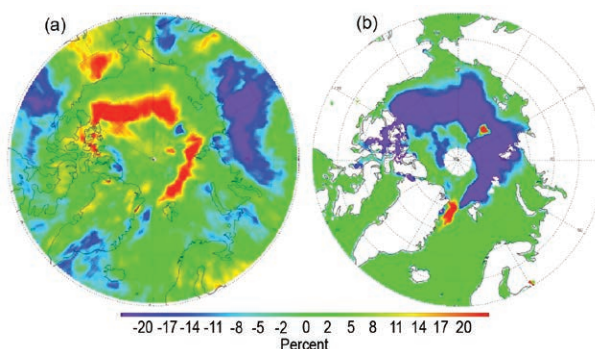


**FIG. 5.4. Cloud cover (a) and sea ice concentration (b) anomalies (in %) in September 2012 relative to the corresponding monthly means for the period 2002–10. (Source: MODIS on the Aqua satellite.)**

## SIDEBAR 5.1: THE EXTREME STORM IN THE ARCTIC BASIN IN AUGUST 2012—I. SIMMONDS

In late summer 2012, a remarkable storm formed over Siberia on 2 August, moved across the Arctic Basin, and finally decayed in the Canadian Arctic Archipelago on 14 August. This cyclone occurred when the sea ice extent was on the way to reaching a new all-time low during the satellite observation era (1979–present; see section 5j), and attracted a great deal of scientific and media interest.

The cyclone has been analyzed using the Melbourne University cyclone tracking scheme (Simmonds and Keay 2002), an algorithm that calculates a broad range of morphological characteristics of the storms it identifies; these include central pressure, radius, depth, vorticity, and lifetime. The scheme was applied to the 6-hourly sea level pressure analyses of the National Centers for Environmental Prediction (NCEP) Climate Forecast System Reanalysis (CFSR; Saha et al. 2010). One of the significant advantages of CFSR for analysis in the polar regions is that it includes atmosphere–ocean coupling, assimilates sea ice concentration data, and is run at high resolution (horizontal: ~38 km; vertical: 64 sigma-pressure hybrid levels).

It is natural to ask what were the connections, if any, between the record low sea ice extent and the occurrence of this intense storm in August 2012? Analysis indicates that the storm behavior was strongly influenced by baroclinicity (as

measured by the Eady growth rate) and by the presence of a long-lived tropopause polar vortex. These are characterized, in part, by the downward intrusion of stratospheric air to about 500 hPa and beyond, and hence have the potential to influence surface development (Kew et al. 2010; Cavallo and Hakim 2012). Baroclinicity was a key factor associated with the rapid decrease in central pressure when the storm crossed into the East Siberian Sea. The surface system formed in a deep southward trough associated with the tropopause polar vortex. After four days, the centers of the tropopause polar vortex and cyclone became vertically aligned, and remained so until the latter's demise over the Canadian Arctic Archipelago.

Detailed analysis reveals that there is little evidence to suggest that the large negative sea ice extent anomaly had any substantial impact on the cyclone (Simmonds and Rudeva 2012). It should be noted that in late summer the surface fluxes of latent and sensible heat (sources of energy for cyclone development) are quite modest, and anomalous sea ice conditions would not be expected to affect these significantly (a different picture of ice–atmosphere interaction would have emerged had this storm occurred in winter).

In contrast, the storm had an immediate and significant effect on the ice distribution. Satellite-based observations indicate

### c. Ozone and UV radiation—G. Bernhard, V. Fioletov, J.-U. GrooB, A. Heikkilä, B. Johnsen, T. Koskela, K. Lakkala, G. Manney, R. Müller, and T. Svendby

Total ozone columns in the Arctic measured by satellites and ground-based instruments during 2012 were, by and large, within the typical range observed during the first decade of the 21st century, but notably below those of the 1979–88 reference period (Fig. 5.5). The 2012 ozone columns were considerably higher than those in the spring of 2011, when unprecedented chemical ozone losses occurred (Manney et al. 2011). The minimum total ozone column for March 2012, averaged over the "equivalent latitude" (Butchart and Remsburg 1986) band 63°N–90°N, was 372 DU (Dobson Units). The 2011 record low was 302 DU. The average for 2000–10 is 359 DU, 13 DU below the value for 2012, and the average for 1979–88 is 397 DU.

Comparing the monthly mean total ozone columns for February–May 2012 compiled by Environment Canada (2013) with data from the reference period 1979–88, notable differences are observed during certain periods and for certain regions.

During February 2012, total ozone at Svalbard was more than 30% below the monthly mean. Regions with monthly mean ozone levels  $\geq 10\%$  below the

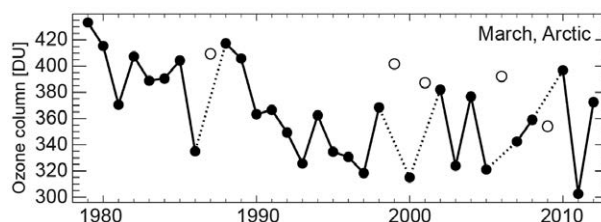
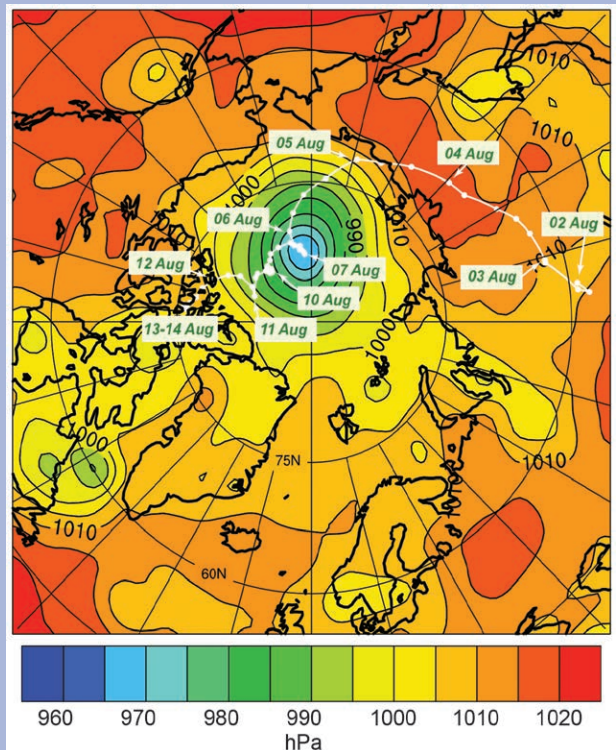


**FIG. 5.5.** Time series of area-averaged minimum total ozone for March in the Arctic, calculated as the minimum of daily average column ozone poleward of 63° equivalent latitude. Winters in which the Arctic vortex broke up before March (1987, 1999, 2001, 2006, and 2009) are shown as open symbols. Ozone in those years was relatively high because of mixing with air from lower latitudes. Figure adapted from Müller et al. (2008), updated using Version 2.8 of the combined total column ozone database produced by Bodeker Scientific (<http://www.bodekerscientific.com/data/total-column-ozone>). The area-averaged minimum total ozone quantity is explained by Müller et al. (2008).

that the storm caused the separation of an expanse of  $0.4 \times 10^6$  km<sup>2</sup> of ice from the main pack, which melted completely and accounted for 57% of the difference between the 2007 and 2012 ice extent minima (Parkinson and Comiso 2013). The loss of this region of ice also left the main pack more exposed to wind and waves, facilitating further decay. Even with this evidence, researchers continue to debate the role the storm played in achieving the record low sea ice extent. For instance, a recent model study by Zhang et al. (2013) suggests that 2012 would have produced a record minimum ice extent without the August storm. More consistent is the expectation that as Arctic sea ice becomes less extensive and thinner it will be more vulnerable to intense storms (e.g., Overeem et al. 2011; Screen et al. 2011; Asplin et al. 2012).

**FIG. SB5.1.** Mean sea level pressure field at 18UTC on 6 August 2012 and the 6-hourly positions of the cyclone from its formation in Siberia (2 Aug) to its demise in the Canadian Arctic Archipelago (14 Aug). The contour interval is 5 hPa. The labels indicate the location of the cyclone at 00UTC on almost every day.



historical reference encompassed the North Pole, the North Sea, northern Siberia, northern Greenland, Scandinavia, Iceland, the British Isles, Denmark, the Netherlands, and northern Germany. Above-average ozone levels were observed over the Aleutian Islands in the North Pacific Ocean. In March, the area with total ozone 10% below the mean was centered on the North Sea and extended towards southern Scandinavia, the British Isles, France, and central Europe. Much of eastern Canada, the eastern United States, and southern Alaska were also affected by below-average total ozone columns. In April, Arctic regions with lower-than-historic ozone included the northern part of Canada (Victoria Island) and southern Greenland. Extended areas with large deviations from the historical measurements were not observed in the Arctic between May and November 2012. Departures from the mean (either up or down) were larger for individual days. For example, deviations exceeding -35% were observed in the western part of Russia as late as the second half of April.

Arctic stratospheric temperatures in December 2011 were among the lowest on record, but rose to near average in late December. The low temperatures facilitated the formation of polar stratospheric clouds (PSC), which play an important role in activating stratospheric chlorine, which then destroys ozone in catalytic cycles. According to data from the Microwave Limb Sounder (MLS) on the Aura satellite, a sudden stratospheric warming in late January 2012 halted PSC formation and hence the activation of chlorine, leading to conditions that did not allow chemical ozone loss to be sustained into spring. Stratospheric ozone concentrations increased slightly through mid-March as vertical motions transported higher ozone down from above.

The distribution of total ozone column over the Arctic on 3 April of the years 1981 (a year with a long-lasting and cold Arctic vortex, and relatively low stratospheric chlorine concentrations), 2002 (long-lasting warm vortex, high total chlorine loading), 2011 (long-lasting cold vortex, high chlorine), and 2012 (warm vortex, high chlorine) is illustrated in

Fig. 5.6. Total ozone was lowest in years when there was a long-lasting, cold vortex, e.g., 2011. Years with a warm vortex, e.g., 2012, resulted in little ozone loss.

UV radiation is expressed as the UV Index, a measure of the ability of UV radiation to cause erythema (sunburn) in human skin (WHO 2002). It is calculated by weighting UV spectra with the action spectrum for erythema (McKinlay and Diffey 1987) and multiplying the result by  $40 \text{ m}^2 \text{ W}^{-1}$ . UV radiation levels measured with ground-based instruments at Arctic locations during the first half of 2012 were generally within the typical range observed during the last two decades, with some notable exceptions. In southern Scandinavia, the UV Index was enhanced between January and March 2012 because the ozone column over this region was significantly below the 1991–2010 mean. For example, the ozone column average for the period January–March 2012 was reduced by 11% over Finse, Norway ( $61^\circ\text{N}$ ,  $8^\circ\text{E}$ ), and by 10% over Østerås, Norway ( $60^\circ\text{N}$ ,  $11^\circ\text{E}$ ). These reductions led to UV Index increases of 11% and 13%, respectively, at these sites. While it is unusual that total ozone remains below the climatological average for three consecutive months, reductions in ozone for individual days and associated enhancements in UV remained, by and large, within historical limits.

The maximum daily UV Index at Barrow, Alaska ( $71^\circ\text{N}$ ,  $157^\circ\text{W}$ ), on 10 June 2012 was 4.8, or 44% (2.3 standard deviations) above the mean value for that day and only 4% below the all-time record of 5.0, measured on 7 June 2000. Total ozone measurements by Ozone Monitoring Instrument (OMI) on 9 June 2012 were as much as 90 DU (26%, 5.2 standard deviations) below the mean value of 341 DU for this day during 1991–2011. Satellite data indicate that the low-ozone event was caused by advection of ozone-poor air from lower latitudes above the contiguous United States. The transport of ozone-poor air from lower to higher latitudes is well documented (e.g., Bojkov and Balis 2001), but advection from subtropical to high latitudes

in June is a rare occurrence on the Pacific side of the Arctic (James 1998; Hood et al. 2001).

*d. Carbon dioxide and methane*—L. Bruhwiler, E. Dlugokencky, T. Laurila, and D. Worthy

Carbon dioxide ( $\text{CO}_2$ ) and methane ( $\text{CH}_4$ ) are responsible for ~82% of direct radiative forcing caused by long-lived greenhouse gases, 2.32 out of  $2.84 \text{ W m}^{-2}$  in 2012 (Hofmann et al. 2006; Butler 2012). Natural emissions of these gases are of particular interest in the Arctic, where there are large, vulnerable reservoirs of carbon and where temperatures have been increasing at a rate roughly twice that observed at lower latitudes (Bekryaev et al. 2010; section 5b). The changing Arctic climate may act as a positive feedback on greenhouse gas emissions from Arctic sources such as the warming tundra and permafrost (e.g., Tarnocai et al. 2009; Schaefer et al. 2011; Harden et al. 2012; Walter Anthony et al. 2012; McGuire et al. 2012) and the seafloor in shallow offshore Arctic waters (Shakhova et al. 2010), further exacerbating global climate change.

Maintaining long observational records is critical to timely detection of Arctic-wide trends in greenhouse gas emissions. The longest time series are from Barrow, Alaska (1983 to present), and Alert, Nunavut, Canada (1985 to present). In total, there are currently 13 operating observation sites (Fig. 5.7) in the Arctic and subarctic regions operated by NOAA, Environment Canada, the Finnish Meteorological Institute, and collaborators in Norway and Iceland. Same-air samples are compared between pairs of institutions, and measurement systems are calibrated against the World Meteorological Programme, Global Atmosphere Watch  $\text{CH}_4$  mole fraction scale helping to ensure consistency among these measurements. For the first time, the atmospheric  $\text{CO}_2$  concentration exceeded 400 ppm in spring 2012 at 7 of these 13 sites.

Detection of trends in greenhouse gas emissions from Arctic sources is difficult because the changes

are expected to be small in comparison to the much larger midlatitude emissions that will eventually find their way into the Arctic atmosphere. The high latitude trend of increasing atmospheric  $\text{CO}_2$  concentration (Fig. 5.8a)

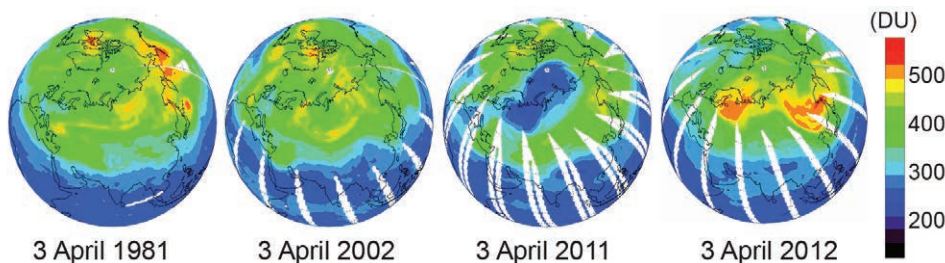


**FIG. 5.6.** Total ozone column (DU) measured by satellites on 3 April 1981, 2002, 2011, and 2012. Data are from the TOMS aboard the *Nimbus-7* (1981) and *Earth Probe* (2002) satellites, and OMI aboard the *Aura* spacecraft (2011 and 2012).

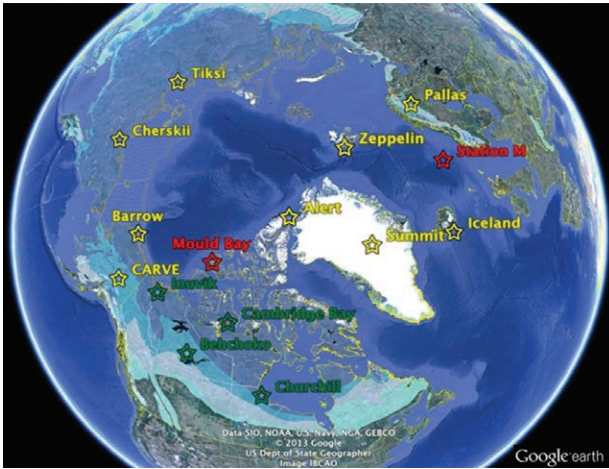


**FIG. 5.7. Sites where atmospheric observations of CO<sub>2</sub>, CH<sub>4</sub>, and other atmospheric trace species are made. Data are no longer collected at sites with red markers. The green markers show sites recently set up by Environment Canada. The observation sites are overlain on the “Circum-Arctic Map of Permafrost and Ground Ice Conditions” (Brown et al. 2001) available from the NSIDC at [http://nsidc.org/data/virtual\\_globes/](http://nsidc.org/data/virtual_globes/).**

is dominated by northward transport of increasing fossil fuel emissions from lower latitudes (the global total emissions from fossil fuel combustion have averaged 8 Pg C yr<sup>-1</sup> over the last decade, while the CO<sub>2</sub> uptake by the high latitude terrestrial biosphere and ocean is about 1 Pg C yr<sup>-1</sup> (<http://www.esrl.noaa.gov/gmd/ccgg/carbontracker>). At present, trends in Arctic atmospheric CO<sub>2</sub> due to changes in Arctic productivity or respiration cannot be distinguished from midlatitude processes, especially from the large emissions from fossil fuel use. The seasonal CO<sub>2</sub> cycle (Fig. 5.8a) reflects uptake by the terrestrial biosphere during the Northern Hemisphere growing season, and respiration during the winter months.

High latitude atmospheric CH<sub>4</sub> concentrations also show a seasonal cycle (Fig. 5.8b), with a summer

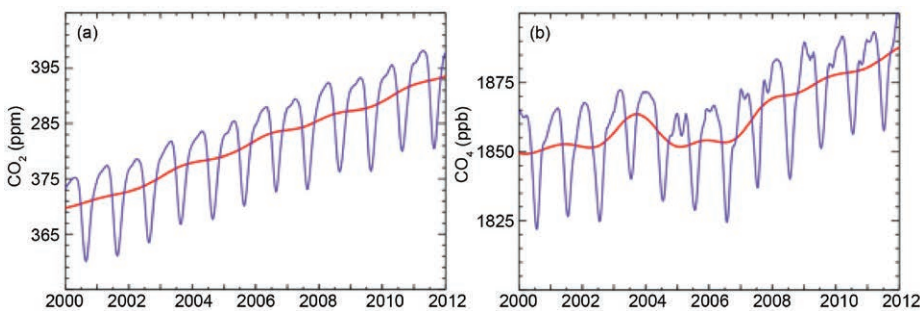


**FIG. 5.8. Zonally-averaged seasonal cycle (blue) and annual average (red) of (a) atmospheric CO<sub>2</sub> concentration and (b) atmospheric CH<sub>4</sub> concentration for ten high-latitude sites between 53°N and 90°N.**

minimum due to solar radiation-dependent photochemical destruction (Fung et al. 1991), and upward trend, particularly since the mid-2000s. The upward trend can be explained by northward transport of changes in emissions at mid- and tropical latitudes since 2007 (Dlugokencky et al. 2009). At present, there is no atmospheric CH<sub>4</sub> evidence for an increase in emissions from Arctic sources such as tundra (McGuire et al. 2012) and offshore areas (Shakhova et al. 2010).

*e. Terrestrial snow*—C. Derksen and R. Brown

Northern Hemisphere spring snow cover extent anomalies (relative to a 1988–2007 reference period) computed from the weekly NOAA snow chart climate data record [CDR; maintained at Rutgers University and described in Brown and Robinson (2011)] for April, May, and June showed a continued reduction from the historical mean during spring 2012 (Fig. 5.9a). New record lows for both May and June snow cover extent (months when snow cover is confined largely to the Arctic) were established over Eurasia in 2012, the fifth consecutive year that a new record low June snow cover extent occurred in this region. Spring 2012 marked the third time in the past five years that a new record low June snow cover extent was set in North America. The rate of snow cover loss over Northern Hemisphere land areas in June between 1979 and 2012 is -17.6% per decade (relative to the 1979–2000 mean), which exceeds the rate of September sea ice loss over the same time period [-13.0% per decade; updated from Derksen and Brown (2012)].

Spatial patterns of fall 2011 and spring 2012 snow cover duration departures derived from the NOAA daily interactive multisensor snow product show near-normal snow cover onset over the Canadian Arctic, earlier-than-normal snow onset across the eastern Siberian Arctic, and later-than-normal snow onset over northern Europe (Fig. 5.9b). The

spring snow cover duration anomaly (Fig. 5.9c) indicates generally earlier snow cover disappearance over Arctic land areas, with the earliest loss of snow cover over the central Canadian Arctic and coastal regions across the Eurasian Arctic. Mean April snow depth from the Canadian Meteorological Centre

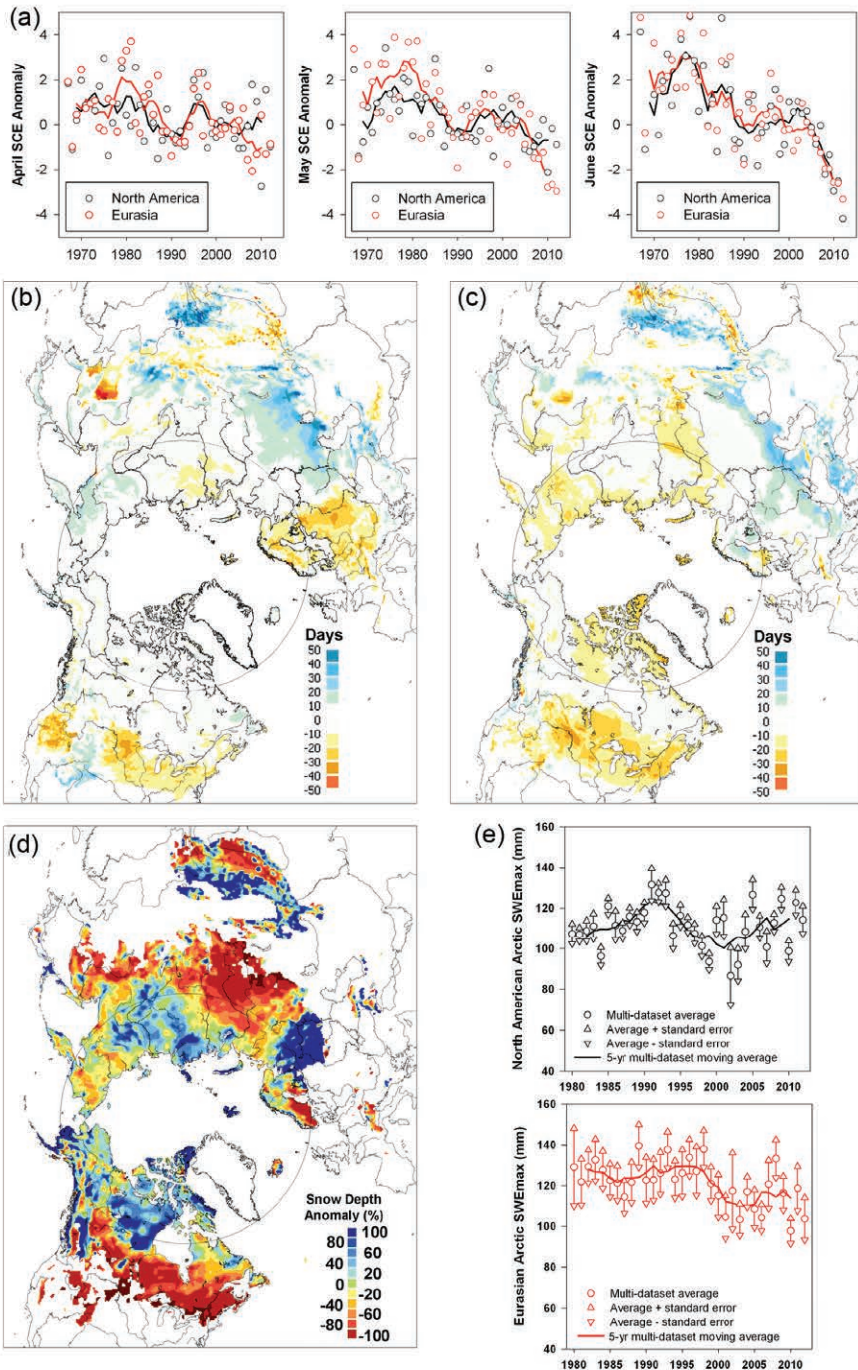


**FIG. 5.9.** (a) Monthly Arctic snow cover extent standardized (and thus unitless) anomaly time series (with respect to 1988–2007) from the NOAA snow chart CDR for Apr, May, and Jun, 1967–2012 (solid lines denote 5-yr moving average); (b) and (c) Snow cover duration departures (with respect to 1998–2010) from the NOAA Interactive Multisensor Snow data record for the 2011 fall season and the 2012 spring season, respectively; (d) Apr 2012 snow depth anomaly (% of 1999–2010 average) from the CMC snow depth analysis; and (e) time series of multidataset average monthly  $SWE_{max}$  standardized anomalies ( $\pm$  the standard error) relative to 1988–2007 (solid lines denote 5-yr moving average).

daily gridded global snow depth analysis (Brasnett 1999) shows large regions of positive April snow depth anomalies over both the North American and Eurasian Arctic (Fig. 5.9d). This suggests the record setting loss of spring snow cover in 2012 was driven by rapid snow ablation rather than anomalously low snow accumulation.

Estimates of historical variability in pan-Arctic maximum seasonal snow water equivalent ( $SWE_{max}$ ) anomalies over land for 1980–2012 were calculated by averaging anomalies from four datasets: (1) GlobSnow, an assimilation of surface observations of snow depth and satellite retrievals from passive microwave data (Takala et al. 2011); (2) a gridded global snow depth analysis based on optimal interpolation of surface snow depth observations (Brasnett 1999; Brown et al. 2003); (3) a snow cover reconstruction driven with temperature and precipitation from the ERA-interim atmospheric reanalysis (Dee et al. 2011); and (4) diagnosed SWE from the MERRA reanalysis (Rienecker et al. 2011). The multidataset anomaly time series for North America (Fig. 5.9e) shows decadal-scale variability with no significant linear trend. The Eurasian  $SWE_{max}$  anomaly for 2012 is consistent with a step change to lower SWE observed since 2000.

Atmospheric circulation during the spring 2012 Arc-

tic snow melt season was characterized by a strongly negative North Atlantic Oscillation (NAO) which reached a low of -2.25 in June (see section 5b). A negative NAO is associated with enhanced southerly air flow into the Arctic which contributes to warm temperature anomalies and rapid ablation of the snowpack. The only other year since 1950 to have a June NAO value lower than -2.0 was 1998 (Atkinson et al. 2006), when warm temperature anomalies were also present across Arctic land areas.

f. *Glaciers and ice caps (outside Greenland)*—G. Wolken, M. Sharp, M-L. Geai, D. Burgess, A. Arendt, and B. Wouters. With data contributions from J. G. Cogley and I. Sasgen.

Mountain glaciers and ice caps cover an area of over 400 000 km<sup>2</sup> in the Arctic, and are a major contributor to global sea level change (Meier et al. 2007; Gardner et al. 2011; Jacob et al. 2012). They gain mass by snow accumulation, and lose mass by surface melt and runoff, and by iceberg calving where they terminate in water (ocean or lake). The climatic mass balance ( $B_{\text{clim}}$ , the difference between annual snow accumulation and annual runoff) is a widely used index of how glaciers respond to climate variability and change.

As  $B_{\text{clim}}$  measurements for the 2011/12 balance year are not yet available, we summarize measurements of 24 Arctic glaciers for 2010/11 (World Glacier Monitoring Service 2013). The glaciers are located in Alaska (three), Arctic Canada (four), Iceland (six), Svalbard (four), Norway (two), and Sweden (five) (Table 5.1). All but three of the glaciers (Dyngjufjökull, Brúarjökull, and Eyjabakkajökull in eastern Iceland) had a negative annual balance (i.e., loss of ice mass). Mass balances of glaciers in Svalbard and northern Scandinavia were very negative in 2010/11. In the Canadian

Arctic, the 2010/11 balances were the most negative on record for all four glaciers. In this region, between five and nine of the most negative mass balance years in the 49–52 year record have occurred since 2000. The mean annual mass balance for the period 2000/11 is between three (Melville South Ice Cap) and eight (Meighen Ice Cap) times as negative as the 1963–99 average for each ice cap. This is a result of strong summer warming over the region that began around 1987 (Gardner and Sharp 2007) and accelerated significantly after 2005 (Sharp et al. 2011). For the monitored Arctic glaciers as a whole, mass balance year 2010/11 continues a trend of increasingly negative cumulative balances (Fig. 5.10).

Trends of increasingly negative cumulative balances are also evident in regional total mass balance estimates ( $\Delta M$ , which includes mass losses by iceberg

**TABLE 5.1. Measured annual climatic mass balances ( $B_{\text{clim}}$ ) of glaciers in Alaska, the Canadian Arctic, Iceland, Svalbard, Norway, and Sweden for 2009/10 and 2010/11. Mass balance data for all glaciers are from the World Glacier Monitoring Service (2013).**

Region	Glacier	Length of Record (yr)	Net Balance 2009/10 (kg m <sup>-2</sup> yr <sup>-1</sup> )	Net Balance 2010/11 (kg m <sup>-2</sup> yr <sup>-1</sup> )
Alaska	Wolverine	46	-85	-1070
	Lemon Creek	59	-580	-720
	Gulkana	46	-1832	-1290
Arctic-Canada	Devon Ice Cap	51	-417	-683
	Meighen Ice Cap	50	-387	-1310
	Melville S. Ice Cap	49	-939	-1339
	White	49	-188	-983
Iceland	Langjökull S. Dome	15	-3800	-1279
	Hofsjökull E	21	-2830	
	Hofsjökull N	22	-2400	
	Hofsjökull SW	21	-3490	
	Köldukvislarjökull	19	-2870	-754
	Tungnaarjökull	20	-3551	-1380
	Dyngjufjökull	14	-1540	+377
	Brúarjökull	19	-1570	+515
	Eyjabakkajökull	20	-1750	+525
Svalbard	Midre Lovénbreen	44	-200	-920
	Austre Broggerbreen	45	-440	-1004
	Kongsvegen	25	+130	-434
	Hansbreen	23	-14	-280
Norway	Engabreen	42	-520	-910
	Langfjordjøkulen	21	-760	-1257
Sweden	Marmaglacieren	22	-500	-1450
	Rabots Glaciar	30	-1080	-2110
	Riukojietna	25	-960	-1080
	Storglacieren	66	-690	-1060
	Tarfalaglacieren	17	-1060	-1820

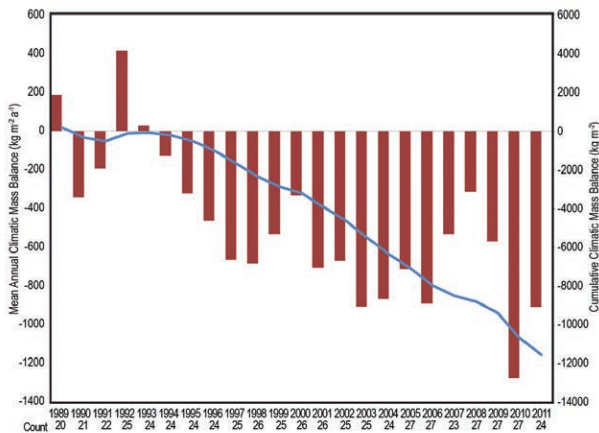


**FIG. 5.10. Mean annual climatic mass balance ( $B_{\text{clim}}$ ) from 1989 to 2011 (red) and cumulative climatic mass balance relative to 1989 (blue) based on available annual measurements (count) for 24 glaciers monitored in the Arctic (World Glacier Monitoring Service 2013).**

calving), derived using GRACE satellite gravimetry (Fig. 5.11). Available for the 2011/12 balance year, estimated  $\Delta M$  of all the glaciers and ice caps in the Canadian Arctic Archipelago (CAA) was  $-106 \pm 27$  Gt, while in the Gulf of Alaska region  $\Delta M$  was  $+51.9 \pm 16.3$  Gt. The CAA estimate matches the record negative value of the previous year (2010/11), and the Gulf of Alaska region estimate is the most positive for the region during the GRACE observation period,

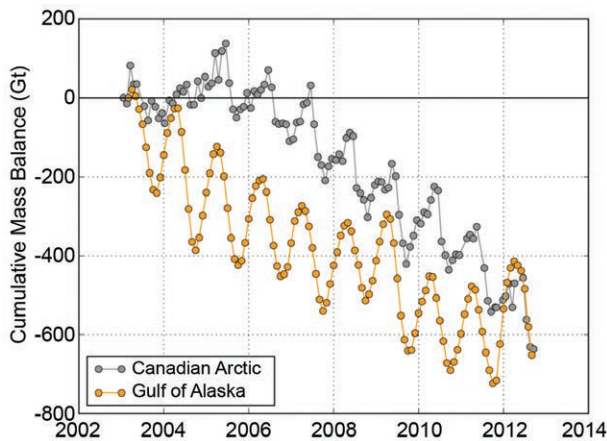


**FIG. 5.11. Cumulative mass balances of Canadian Arctic Archipelago (CAA) and Gulf of Alaska region (GoA) glaciers, determined from the GRACE satellites. CAA data are unpublished estimates derived from monthly Stokes coefficients from the Center for Space Research fifth release (CSR RL5) and processed following methods in Gardner et al. (2011) and Wouters and Schrama (2007). The GoA data are unpublished estimates updated from Sasgen et al. (2012) and derived from a composite of monthly Stokes coefficients from the CSR, the Jet Propulsion Laboratory, and the German Research Center for Geosciences processing centers.**

2003–12 (Fig. 5.11). The higher rates of mass loss in the CAA (Fig. 5.11), and the strongly negative  $B_{\text{clim}}$  values reported in the previous paragraph, confirm the growing importance of glaciers and ice caps in this region as contributors to global sea level rise (Gardner et al. 2011).

Variability in mean summer temperature accounts for much of the interannual variability in  $B_{\text{clim}}$  in cold, dry regions like the Canadian high Arctic while, in more maritime regions, like Iceland and the Gulf of Alaska region, variability in winter precipitation is also a factor. Land surface temperature (LST) over ice in summer may serve as a proxy for  $B_{\text{clim}}$  of glaciers across the Arctic. Moderate to large positive LST anomalies over glaciers and ice caps occurred throughout the Arctic during summer 2012, particularly in the Canadian high Arctic (Fig. 5.12). Summer mean LSTs in 2012 were the warmest in the 13-year record on northern Ellesmere and Agassiz ice caps—exceeding the record set the previous year—and the second warmest on the Axel Heiberg Island, Prince of Wales (eastern Ellesmere Island), and Penny (southern Baffin Island) ice caps. Elsewhere in the Arctic, summer mean LSTs in 2012 equaled the 2011 record on Franz Josef Land, and were the second and fourth warmest in Severnaya Zemlya and Novaya Zemlya, respectively. In contrast, 2012 summer mean LSTs were only the eighth warmest in the 13-year long record in Iceland and the tenth warmest in southern Alaska (Fig. 5.12), where  $B_{\text{clim}}$  and  $\Delta M$ , respectively, were positive.

Data from the NCEP/NCAR R1 reanalysis were also used as indicators of climatic conditions over the major glaciated regions of the Arctic during the 2011/12 mass balance year. Relative to the 1948–2008

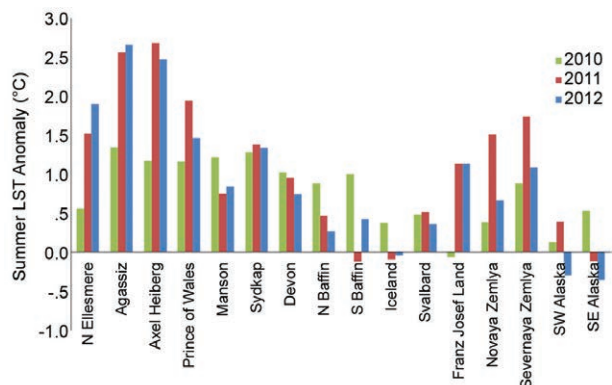


**FIG. 5.12. Comparison of 2010, 2011, and 2012 summer mean land surface temperature (LST) anomalies (relative to 2000–10) for 16 glaciated regions of the Arctic based on the MODIS MOD11A2 LST product (ORNL DAAC 2010).**

mean, winter (September 2011–May 2012) precipitation was significantly above normal in southern Alaska and Iceland (see Fig. 5.9) and near normal elsewhere in the Arctic. Summer air temperature anomalies (JJA 2012 mean at 700 hPa geopotential height, relative to the 1948–2008 mean) were again strongly positive (+1.4°C to +3.6°C) over the Canadian Arctic Islands (including Baffin Island), and positive over Severnaya Zemlya (+0.41°C) and Franz Josef Land (+0.48°C). They were close to normal in Svalbard, Iceland, and southern Alaska. These patterns are broadly consistent with the pattern of summer LST anomalies and glacier mass balance.

The region of strongly positive summer 700 hPa air temperature anomalies in 2012 over south and west Greenland, Baffin Island, and Canada’s Queen Elizabeth Islands is associated with a region of anomalously high geopotential height at all levels of the troposphere that was centered over Greenland and Baffin Bay. (Figure 5.3b shows the anomalously high pressure in this region.) This is a feature that has persisted during summers of the last six years (Box et al. 2012a; Sharp et al. 2011). These positive anomalies point to another strong melt season on these ice caps in 2012, and it is worth noting that the extreme warm temperature event of 8–12 July 2012 that produced record melt extent on the Greenland Ice Sheet (Box et al. 2012a; section 5g) also affected the ice caps in Arctic Canada. In contrast, the near-normal summer air temperatures in Iceland and southern Alaska (where summer LST anomalies were negative), followed heavy winter precipitation in 2011/12, and may therefore have resulted in relatively low summer melt in those regions in 2012.

g. *Greenland Ice Sheet*—M. Tedesco, P. Alexander, J. E. Box, J. Cappelen, T. Mote, K. Steffen, R. S. W. van de Wal, J. Wahr, and B. Wouters

1) **SATELLITE OBSERVATIONS OF SURFACE MELTING AND ALBEDO**

Melting at the surface of the Greenland Ice Sheet set new records for extent and melt index (i.e., the number of days on which melting occurred multiplied by the area where melting was detected) for the period 1979–2012, according to passive microwave observations (e.g., Tedesco 2007, 2009; Mote and Anderson 1995). Melt extent reached ~97% of the ice sheet surface during a rare, ice-sheet-wide event on 11–12 July (Fig. 5.13a; Nghiem et al. 2012). This was almost four times greater than the average melt extent for 1981–2010. The 2012 standardized melting index (SMI, defined as the melting index minus its

average and divided by its standard deviation) was +2.4, almost twice the previous record of about +1.3 set in 2010 (Fig. 5.13b).

According to satellite observations, melting in 2012 began about two weeks earlier than average at low elevations, and lasted as much as 140 days (20–40 days greater than the mean value) in some areas of southwest Greenland (section 5e). Melting day anomalies (i.e., the number of melting days in 2012 minus the 1980–2010 average) were as much as +27 days in the south and +45 days in the northwest. Areas in northwest Greenland between 1400 m and 2000 m above sea level (a.s.l.), where melting is expected to be negligible or sporadic, experienced nearly two months longer melt duration in 2012 than the 1981–2010 reference period.

The area-averaged albedo of the ice sheet, estimated from spaceborne observations (MODIS), set a new record in 2012 (Fig. 5.14a). Negative albedo anomalies were widespread across the ice sheet, but were particularly low along the western and northwestern margins (Fig. 5.14b). The lowest albedo values occurred in the upper ablation zone and overlapped with the regions of extended melt duration.

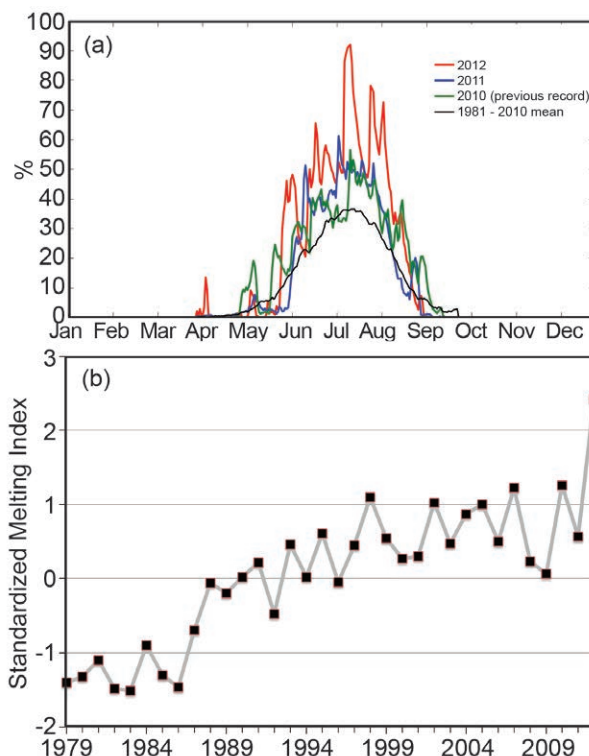


**FIG. 5.13. (a) Surface melt extent, detected by the SSM/I passive microwave sensor, expressed as % of the total area of the Greenland Ice Sheet. (b) Standardized melt index (SMI) for the period 1979–2012 using the Tedesco (2009) algorithm.**

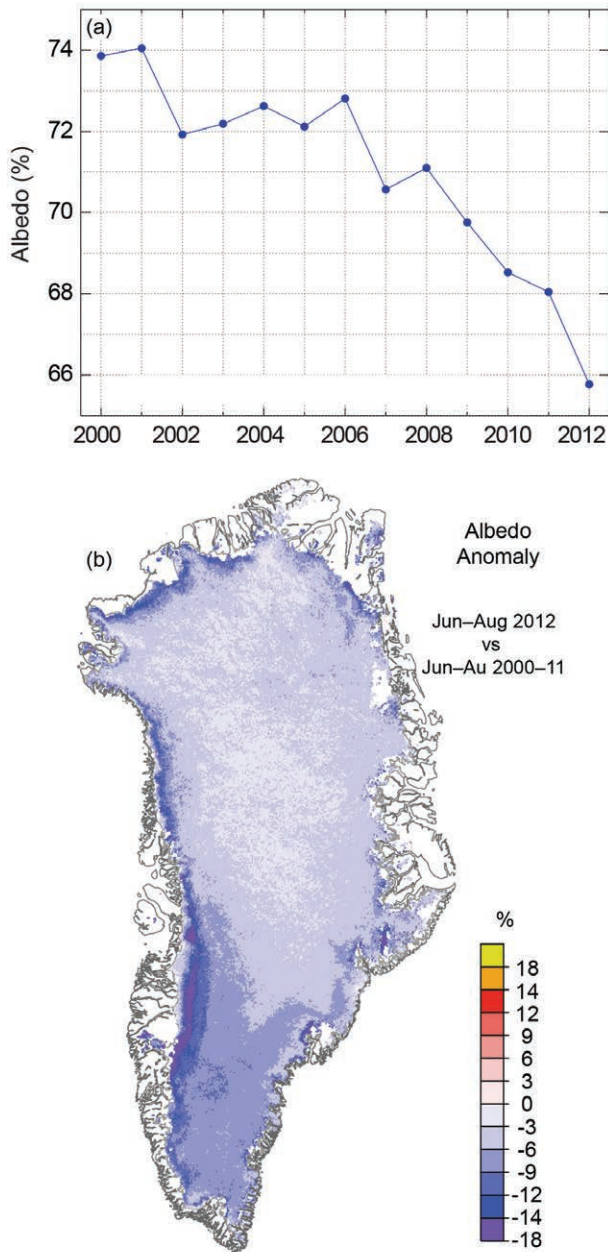


**FIG. 5.14. (a) Area-averaged albedo of the Greenland Ice Sheet each Jul from 2000 to 2012, and (b) geographic variability of the Jun–Aug 2012 albedo anomaly expressed as % of the mean anomaly of the 2000–11 reference period. All data are derived from MODIS MOD10A1 observations. Figures are after Box et al. (2012b).**

## 2) SATELLITE OBSERVATIONS OF ICE MASS LOSS

In 2012, new records for summertime and annual ice mass loss, as estimated from the GRACE satellite mission (e.g., Velicogna and Wahr 2006), occurred. Between June and August, the mass loss was  $-627 \pm 89$  Gt, 2 standard deviations below the 2003–12 mean of  $-414$  Gt (Fig. 5.15; Tedesco et al. 2012). The previous

record mass loss,  $-516 \pm 89$  Gt, 0.8 standard deviation below the mean, occurred in 2010. The trend of summer mass change during 2003–12 is  $-29 \pm 11$  Gt  $\text{yr}^{-1}$ . Excluding the mass loss in summer 2012, the trend is  $-20 \pm 13$  Gt  $\text{yr}^{-1}$ . The annual mass loss from mid-September 2011 to mid-September 2012,  $-575 \pm 89$  Gt, 2 standard deviations below the mean, also set a new record, exceeding the previous record, set only two years earlier, by  $+152$  Gt.

## 3) SURFACE MASS BALANCE OBSERVATIONS ALONG THE K-TRANSECT

The original K-Transect is located in western Greenland near Kangerlussuaq at  $67^\circ\text{N}$  and between 340 m and 1500 m a.s.l. (van de Wal et al. 2005). During the period 1991–2012, 1500 m a.s.l. was the average equilibrium line altitude (ELA; i.e., the highest altitude at which winter snow survives). In 2012, the ELA reached 2687 m a.s.l., 3.7 standard deviations above the mean (van de Wal et al. 2012). The surface mass balance in 2012, between 340 m and 1500 m a.s.l., was the second lowest since measurements began in 1991. However, a weighted mass balance that includes a site above the former 1500 m ELA indicates that the 2011/12 mass balance year was the most negative in 21 years. At the highest station in 2012, 1847 m, almost 350 m higher than the former ELA, the surface mass balance was estimated to be  $-0.74$  m water equivalent. Below 1500 m elevation, surface mass balance values decreased gradually to normal values near the ice margin.

## 4) SURFACE AIR TEMPERATURE OBSERVATIONS

The extensive surface melting and ice mass loss observed in 2012 occurred in conjunction with record summer (June, July, and August: JJA) air temperatures. The ice sheet-wide JJA surface temperature estimated from space by MODIS increased

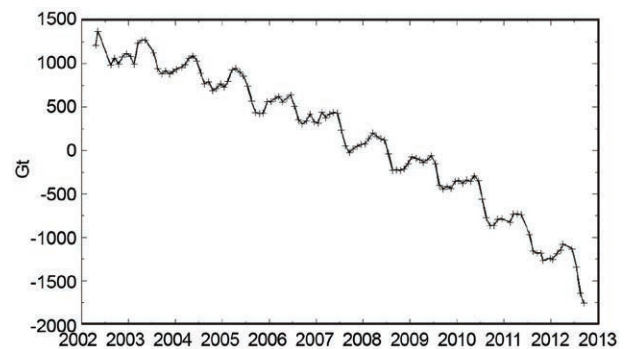


**FIG. 5.15. Cumulative mass anomaly in Gt of the Greenland Ice Sheet derived from GRACE satellite data between April 2002 and September 2012.**

3.4°C between 2000 and 2012, from an average value of -9°C in 2000 to -5.6°C in 2012 (Tedesco et al. 2012). Applying a linear fit, this suggests an increase in ice sheet-wide surface temperature of +0.16°C yr<sup>-1</sup>. Other than Tasiilaq, in southeast Greenland, where June 2012 was the coldest it had been since records began in 1895, record-setting warm JJA surface air temperatures occurred at long-term meteorological stations (records began in 1873) along the western and southern margins of the island and at the ice sheet summit. The Greenland Climate Network (GC-Net) automatic weather station at Summit (3199 m a.s.l.) measured hourly-mean air temperatures above 0°C for the first time since measurements began in 1996. Such a melt event is rare; the last significant event occurred in 1889, according to the analysis of ice core data (Nghiem et al. 2012).

Seasonally-averaged upper air temperature data available from twice-daily radiosonde observations show anomalous warmth throughout the troposphere in summer 2012 (section 5f). This is consistent with an overall warming pattern near the surface between 850 hPa and 1000 hPa. The recent warming trend is seen in the long-term air temperature reconstruction for the ice sheet, which also shows that mean annual air temperatures in all seasons are now higher than they have been since 1840 (Box et al. 2012a).

##### 5) MARINE-TERMINATING GLACIERS

Forty marine-terminating glaciers have been surveyed daily since 2000 using cloud-free MODIS visible imagery (Box and Decker 2011; <http://bprc.osu.edu/MODIS/>). The net area change of the 40 glaciers during the period of observation has been -1775 km<sup>2</sup>, with the 18 northernmost (>72°N) glaciers alone contributing to half of the net area change. In 2012, the northernmost glaciers lost a collective area of 255 km<sup>2</sup>, or 86% of the total net area change of the 40 glaciers surveyed. The six glaciers with the largest net area loss in 2012 were Petermann (-141 km<sup>2</sup>), 79 glacier (-27 km<sup>2</sup>), Zachariae (-26 km<sup>2</sup>), Steenstrup (-19 km<sup>2</sup>), Steensby (-16 km<sup>2</sup>, the greatest retreat since observations began), and Jakobshavn (-13 km<sup>2</sup>). While the total area change was negative in 2012, the area of four of the forty glaciers did increase relative to the end of the 2011 melt season. The anomalous advance of these four glaciers is not easily explained, as the mechanisms controlling the behavior of individual glaciers are uncertain due to their often unique geographic settings.

*h. Permafrost*—V. E. Romanovsky, A. L. Kholodov, S. L. Smith, H. H. Christiansen, N. I. Shiklomanov, D. S. Drozdov, N. G. Oberman, and S. S. Marchenko

Systematic observations of permafrost temperature at many sites in Alaska, Canada, and Russia since the middle of the 20th century provide several decades of continuous data, which allow decadal changes in permafrost temperatures to be assessed. A general increase in temperatures has been observed during the last several decades in Alaska, northern Canada, and Siberia (Smith et al. 2010; Romanovsky et al. 2010a,b). During the last four to five years, all these regions show similar temporal and spatial variability of permafrost temperature. As illustrated for selected sites in Russia (Fig. 5.16), although temperature has been generally increasing continuously in colder permafrost located close to the Arctic coasts (Romanovsky et al. 2012a), the temperatures of warmer permafrost in the continental interior have been relatively stable or even decreasing slightly. Permafrost temperature has increased by 1°C–2°C in northern Russia during the last 30 to 35 years, but this trend was interrupted by colder conditions in summer 2009 and winters 2009/10 and 2010/2011 at many locations in the Russian Arctic, especially in the western sector (Fig. 5.16). However, the warming trend resumed in 2012.

In 2012, new record high temperatures at 20-m depth were measured at most permafrost observatories on the North Slope of Alaska, i.e., north of the Brooks Range (Fig. 5.17a), where measurements began in the late 1970s. The exceptions were the coastal sites, West Dock, and Deadhorse (Fig. 5.17b), where temperatures in 2012 were the same as the record-high temperatures observed in 2011 (Fig. 5.17b). Changes in permafrost temperatures at 20-m depth are typically lagging by one year compared to the changes in surface temperatures. The data suggest that a coastal warming trend has propagated southward towards the northern foothills of the Brooks Range, where a noticeable warming in the upper 20 m of permafrost has become evident since 2008 (Romanovsky et al. 2012b). Record high temperatures were also observed in 2012 in the Brooks Range (Chandalar Shelf) and in its southern foothills (Coldfoot). However, permafrost temperatures in Interior Alaska (e.g., Healy, Birch Lake, College Peat, and Old Man; Fig. 5.17c) were still decreasing in 2012. These distinct patterns of permafrost warming on the North Slope and a slight cooling in the Alaska Interior in 2010–11 are in good agreement with air temperature patterns observed in the Arctic and the sub-Arctic over the last five years

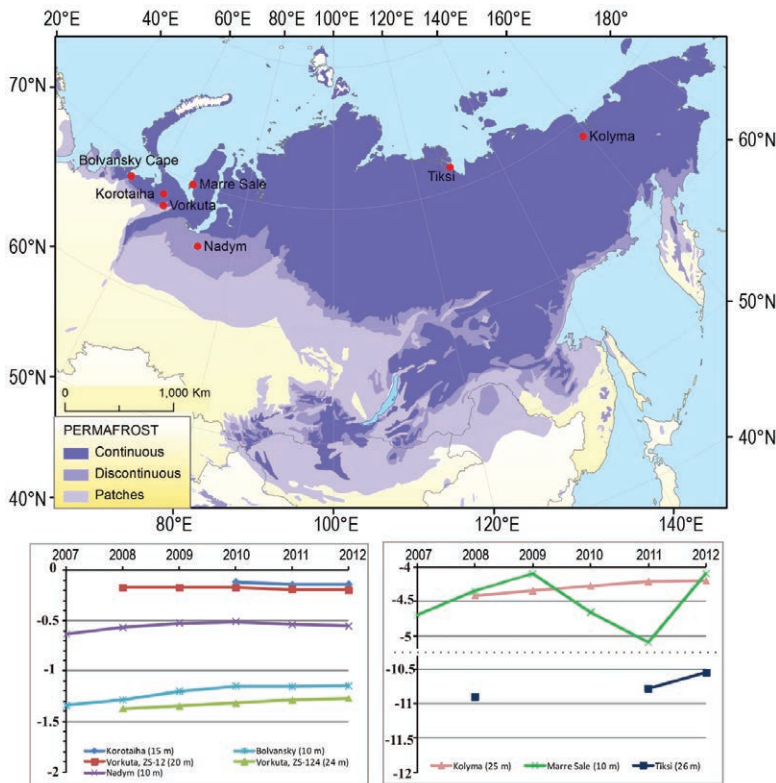


**FIG. 5.16. (Top) Location of selected Russian permafrost temperature observation sites. Measurements during the last five years: (bottom left) at 10-m to 24-m depth in the discontinuous permafrost zone, and (bottom right) at 10-m to 26-m depth in the continuous permafrost zone of Russia. Note, each graph has a different temperature scale; consequently, temperatures are higher in the discontinuous zone (bottom left) due to much warmer climatic conditions compared to the continuous permafrost zone (bottom right).**

and might also be a result of snow distribution variations (Romanovsky et al. 2012a).

In northwestern Canada, cold permafrost temperature has increased during the last 40 years (Burn and Kokelj 2009). Smaller increases in permafrost temperature have been observed for warm permafrost of the discontinuous zone, where recent data indicate a negligible change, ( $<0.2^{\circ}\text{C decade}^{-1}$ ; Romanovsky et al. 2012a; Smith et al. 2010). At Alert ( $82.5^{\circ}\text{N}$ , northernmost Ellesmere Island) in the high Canadian Arctic, greater warming has been observed, with recent data indicating that the steady increase in permafrost temperature since 2000 is continuing largely in response to increasing winter air temperature (Romanovsky et al. 2012a; Smith et al. 2012). Long-term permafrost temperature records are limited for the Nordic area, where a few began at the end of the 1990s. These show recent decadal warming of  $0.04^{\circ}\text{C}-0.07^{\circ}\text{C yr}^{-1}$  in the highlands of southern Norway, northern Sweden, and Svalbard, with the

largest warming in Svalbard and in northern Scandinavia (Isaksen et al. 2011; Christiansen et al. 2010).

Decadal trends in the active layer thickness (ALT) vary by region (Shiklomanov et al. 2012). A progressive increase in ALT has been observed in some Nordic countries, e.g., in the Abisko area of Sweden since the 1970s, with a higher rate after 1995, resulting in the disappearance of thin permafrost in several mire landscapes (e.g., Åkerman and Johansson 2008; Callaghan et al. 2010). This increase ceased during 2007–10, coincident with drier summer conditions (Christiansen et al. 2010). Active layer thickness increased since the late 1990s on Svalbard and Greenland, but the rates vary spatially and temporarily (Christiansen et al. 2010). An increase in ALT over the last fifteen years has been observed in the north of Russian Europe (Drozdov et al. 2012; Kaverin et al. 2012), but ALT was relatively stable in the north of West Siberia. On the North Slope of Alaska ALT is relatively stable, without pronounced trends during 1995–2008 (Streletskiy et al. 2008; Shiklomanov et al. 2010). Similar results are reported from the western Canadian Arctic. Smith et

al. (2009) found no definite trend in the Mackenzie Valley during the last 15 years, with some decrease in ALT following a maximum in 1998. In the eastern Canadian Arctic, ALT increased since the mid-1990s, with the largest increase occurring in bedrock of the discontinuous permafrost zone (Smith et al. 2010).

*i. Lake ice*—C. R. Duguay, L. Brown, K.-K. Kang, and H. Kheyrollah Pour

Ice cover plays a significant role in lake-atmosphere interactions at high latitudes. Its presence or absence influences regional weather and climate (Kheyrollah Pour et al. 2012). Freeze-up (ice-on) and break-up (ice-off) dates, and ice cover duration, commonly referred to as ice phenology, are robust indicators of climate variability and change (e.g., Brown and Duguay 2010). There is ample evidence that the timing of freeze-up/break-up dates and ice cover duration are particularly sensitive to air temperature changes (Jeffries et al. 2012). Analysis of

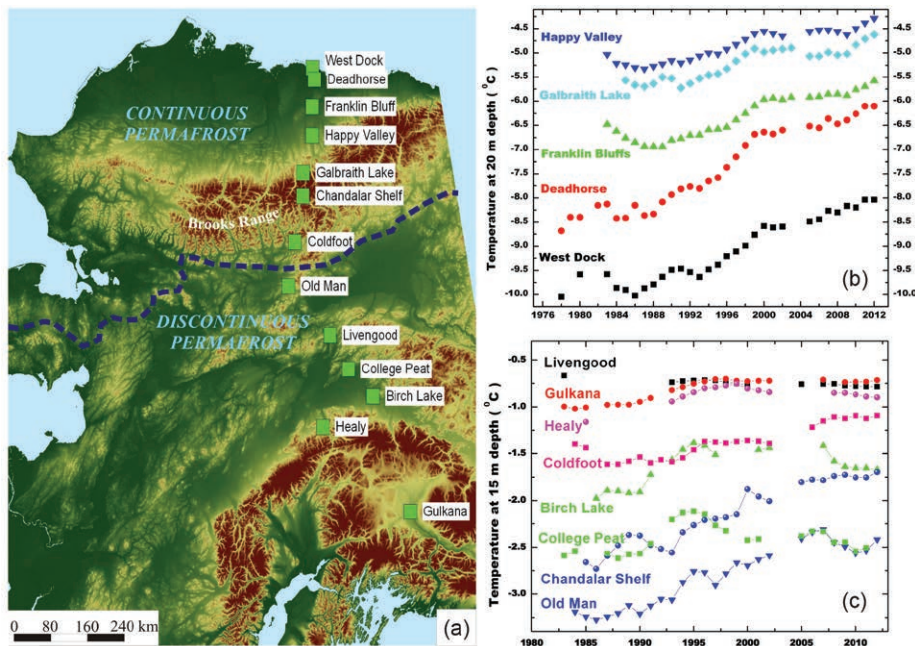


**FIG. 5.17. (a) Map of Alaska showing the continuous and discontinuous permafrost zones (separated by the broken blue line) and location of a north-south transect of permafrost temperature measurement sites; (b) and (c) time series of mean annual temperature at depths 20 m and 15 m below the surface, respectively.**

limited in situ and satellite records (1950s–2004) from northern Canada shows increasingly later freeze-up and earlier break-up dates and, consequently, shorter ice cover duration (Duguay et al. 2006; Latifovic and Pouliot 2007). Although ice cover duration over the Arctic has decreased significantly, largely in response to increasingly warmer conditions during the 20th century, the patterns have varied regionally, primarily due to climate impacts associated with large-scale atmospheric and oceanic oscillations (e.g. Prowse et al. 2011). Ice year 2011/12 provides a good illustration of the influence of teleconnection patterns on the ice regime of Arctic lakes.

Freeze-up and break-up dates, and ice cover duration were derived at the grid-cell level for the largest lakes of the Arctic (4 km × 4 km or larger) using the NOAA Interactive Multisensor Snow and Ice Mapping System 4 km resolution daily product (National Ice Center 2008) for the complete length of the available record (2004–12). (See Helfrich et al. 2007 for details). Freeze-up, break-up, and ice cover duration anomalies (expressed as number of days) between ice year 2011/12 and mean conditions for the reference period 2004–10 were then calculated.

Freeze-up in 2011/12 was earlier than the 2004–11 mean by 10–30 days in eastern and part of central Arctic Canada, Norway, and eastern Siberia (Fig. 5.18a). Freeze-up occurred almost a full month later

for most lakes located in the southern portion of northern Europe. The positive North Atlantic Oscillation (NAO) of fall 2011 and winter 2012 (section 5b) was the likely cause for the late freeze-up in the latter region and early freeze-up in the Canadian Arctic. A positive NAO is associated with higher temperatures over Europe and lower-than-normal values over northeastern Canada. The NAO has previously been shown to affect lake ice phenology in northeastern Canada, Scandinavia, and northwestern Russia (Bonsal et al. 2006).

With few exceptions,

break-up in 2012 occurred several days earlier in Arctic Canada and Eurasia compared to the 2004–11 mean (Fig. 5.18b). Break-up dates were, on average, as much as 3 weeks earlier throughout Arctic Canada and up to 1 month earlier in Eurasia. The few lakes that experienced later break-up (e.g., southern portion of northern Europe) showed small deviations from the mean (1 week on average). The earlier break-up in eastern Siberia and much of Arctic Canada is consistent with the record-low June 2012 snow cover extent (section 5e). The strong negative NAO of spring and summer 2012 (section 5b), which promoted southerly air flow into the Arctic, had a significant impact on lake ice break-up dates and other components of the cryosphere (sections 5e, 5g).

Compared to the 2004–11 mean, ice cover duration in 2011/12 was ~2–5 weeks shorter in central Arctic Canada, western Siberia, southern Scandinavia, and parts of northwestern Russia. On the other hand, ice cover duration was 1–4 weeks longer in eastern Arctic Canada (i.e., Baffin Island and both sides of near-coastal regions of northern Hudson Bay) and 1–8 weeks longer in Norway (Fig. 5.18c). Longer ice cover duration in the northeastern Canadian Arctic and shorter ice duration in northern Eurasia is typically associated with positive phases of the NAO (Prowse et al. 2011).

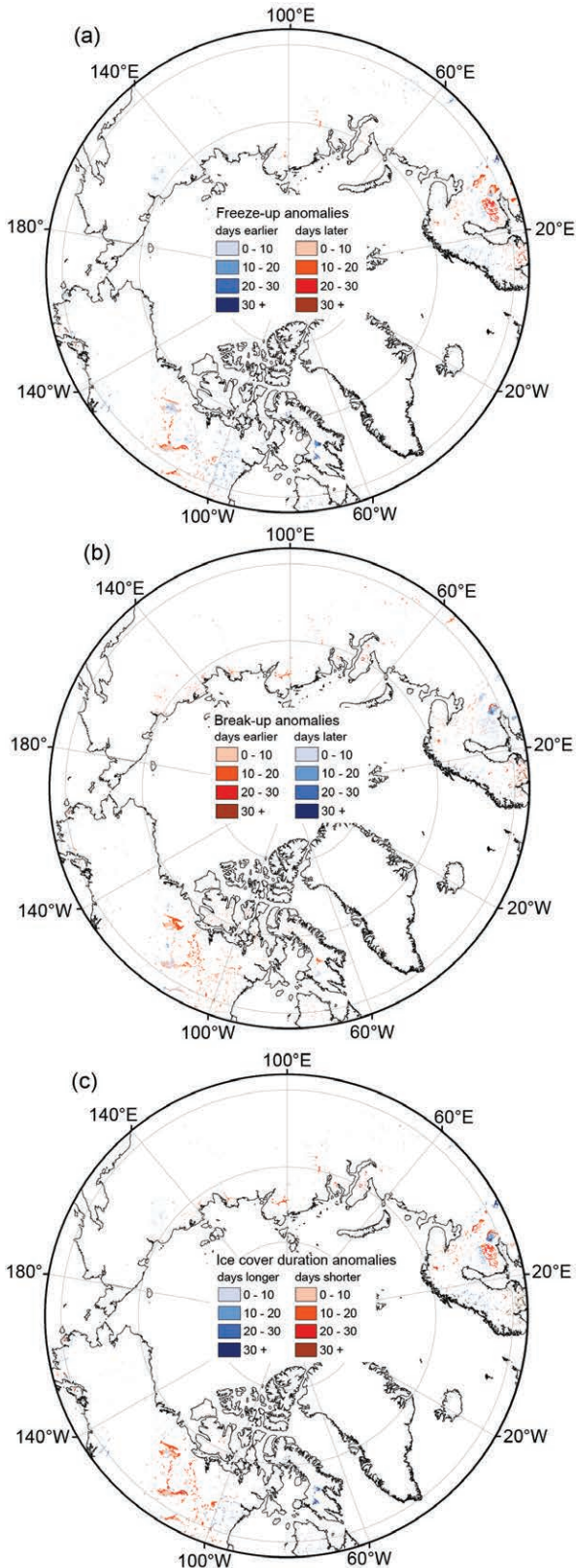


**FIG. 5.18.** (a) Freeze-up, (b) break-up, and (c) ice cover duration anomalies in 2011/12 relative to the 2004–11 reference period from the NOAA Interactive Multi-sensor Snow and Ice Mapping System 4 km product.

j. Sea ice cover—D. K. Perovich, W. Meier, M. Tschudi, S. Gerland, and J. Richter-Menge

1) SEA ICE EXTENT

There is an accurate record of sea ice extent determined from satellite-based passive microwave instruments since 1979. There are two months each year that are of particular interest: September, at the end of summer, when the ice reaches its annual minimum extent, and March, at the end of winter, when the ice is at its maximum extent. Ice extent in March 2012 and September 2012 are illustrated in Fig. 5.19.

Based on estimates by the National Snow and Ice Data Center, on 16 September 2012, the sea ice cover reached its minimum extent for the year of 3.41 million km<sup>2</sup>. This was the lowest in the satellite record, 18% lower than in 2007, when the previous record of 4.17 million km<sup>2</sup> was recorded (Fig. 5.20). Overall, the 2012 minimum was 3.29 million km<sup>2</sup> (49%) below the 1979–2000 average minimum of 6.71 million km<sup>2</sup>. The last six years, 2007–12, have the six lowest minimum extents since satellite observations began.

In March 2012 ice extent reached a maximum value of 15.24 million km<sup>2</sup> (Fig. 5.20), 4% below the 1979–2000 average. Although this was the highest maximum in nine years, the period 2004–12 has the nine lowest maximum extents since 1979. The relatively large maximum extent in March 2012 was due to conditions in the Bering Sea, where ice extent was at or near record levels throughout the winter and spring.

After reaching maximum extent, the seasonal decline began slowly, particularly in the Bering Sea, and around mid-April extent was close to the 1979–2000

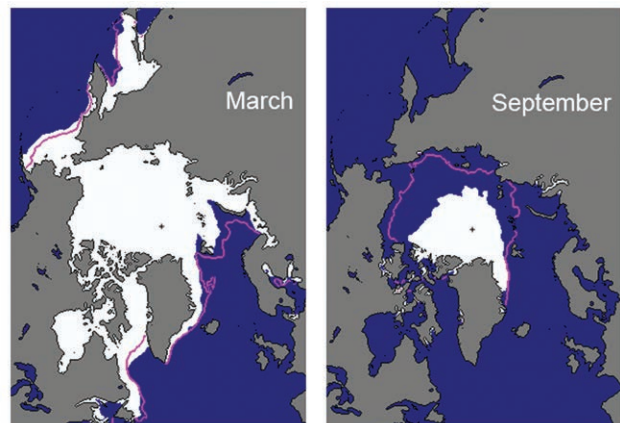


**FIG. 5.19.** Sea ice extent (in white) in Mar 2012 and Sep 2012, the winter maximum and summer minimum, respectively. The magenta line shows the median maximum and minimum ice extents in Mar and Sep for the period 1979–2000. (Source: NSIDC Sea Ice Index, [http://nsidc.org/data/seaice\\_index](http://nsidc.org/data/seaice_index).)

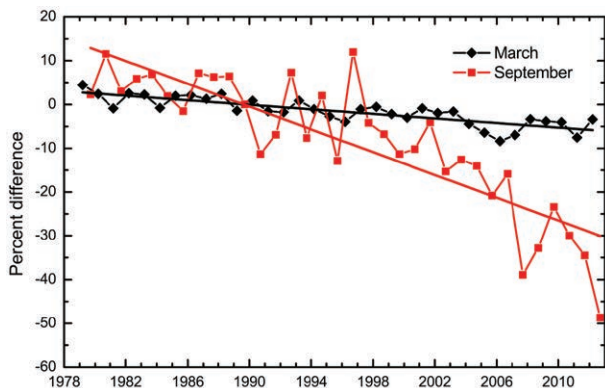


**FIG. 5.20.** Time series of ice extent anomalies in Mar (the month of ice extent maximum) and Sep (the month of ice extent minimum) in % relative to the mean value for 1979–2000. The black and red lines are least squares linear regression lines with slopes indicating ice losses of -2.6% and -13.0% per decade in Mar and Sep, respectively.

average for the time of year. However, soon after that the decline accelerated and was faster than any summer retreat on record. August 2012 was a period of particularly rapid ice loss, in part due to the cyclone that passed through the region at the beginning of the month (Sidebar 5.1). Overall, 11.83 million km<sup>2</sup> of ice was lost between the maximum and minimum extents. This is the largest seasonal decline in the record and 1 million km<sup>2</sup> less ice than in any previous year.

Sea ice extent has decreasing trends in all months and virtually all regions (the exception being the Bering Sea during winter). The September monthly average trend is now -91 600 km<sup>2</sup> per year or -13.0% per decade relative to the 1979–2000 average (Fig. 5.20). The magnitude of the trend has increased every year since 2001. Trends are smaller during March, but still decreasing and statistically significant. The March trend is -2.6% per decade.

Four time periods of the average ice extent for each month are compared in Fig. 5.21: the reference period 1979–2000, 2001–06, the last six years (2007–12) beginning with the previous record minimum of 2007, and 2012. The 1979–2000 period has the largest ice extent for every month, with the greatest difference between the time periods occurring in September. Comparing the two 21st century periods shows that ice extent is similar in winter and spring, but summer values are significantly lower in 2007–12. Figure 5.21 also emphasizes how extreme the ice retreat was in summer 2012.

## 2) SPATIAL DISTRIBUTION OF SEA ICE

In 2007, when the previous record minimum extent occurred, persistent winds through the sum-

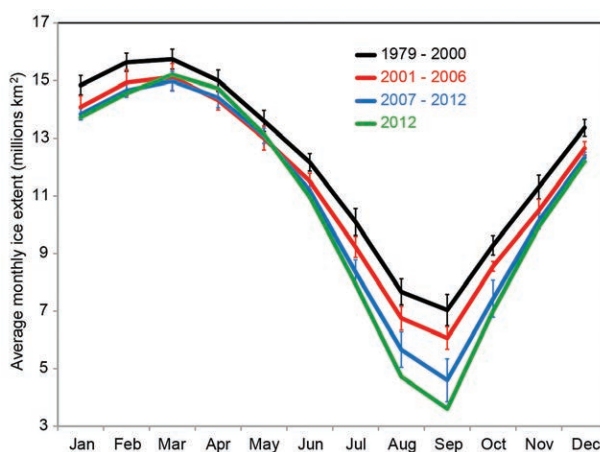


**FIG. 5.21.** Mean monthly sea ice extent for 2012 and three periods: the reference period 1979–2000, 2001–06, and 2007–12. The vertical bars represent one std dev about the mean value for each month.

mer, created by an Arctic dipole circulation pattern (see Arctic Report Card 2007, figure A3), resulted in a compact ice cover and an ice edge far to the north on the Pacific side of the Arctic. However, the circulation also pushed ice onto the coast in the Laptev Sea, completely blocking the Northern Sea Route. In the years since 2007, the pattern of ice loss has varied, but a tongue of older ice in the East Siberian Sea has persisted through the summer (Fig. 5.22). This tongue was particularly evident in 2010 and 2011. In 2012, that tongue of ice mostly melted away, aided by the August storm (Sidebar 5.1), and ice retreated significantly around the entire perimeter of the ice pack (Fig. 5.19, right). This includes the Atlantic side, north of Svalbard, where extents had been near normal in recent years. Overall, compared to 2007 there was more ice in 2012 in the central Arctic north of the Bering Strait, but less ice nearly everywhere else.

A major storm that moved across the Arctic Basin in early August 2012 (Sidebar 5.1) accelerated ice loss in the Chukchi and East Siberian Seas and helped to quickly remove ice from the region. The storm blew the mostly first-year ice southward into warmer water, where satellite observations indicated that it melted in a few weeks (Parkinson and Comiso 2013). As the ice melted and diverged, ice concentration quickly fell below the detection limit of passive microwave sensors, though small amounts of ice were observed for a couple of weeks afterwards by operational ice analysts using other imagery.

## 3) SEA ICE AGE

The age of the ice is another key descriptor of the state of the sea ice cover. Older ice tends to be thicker

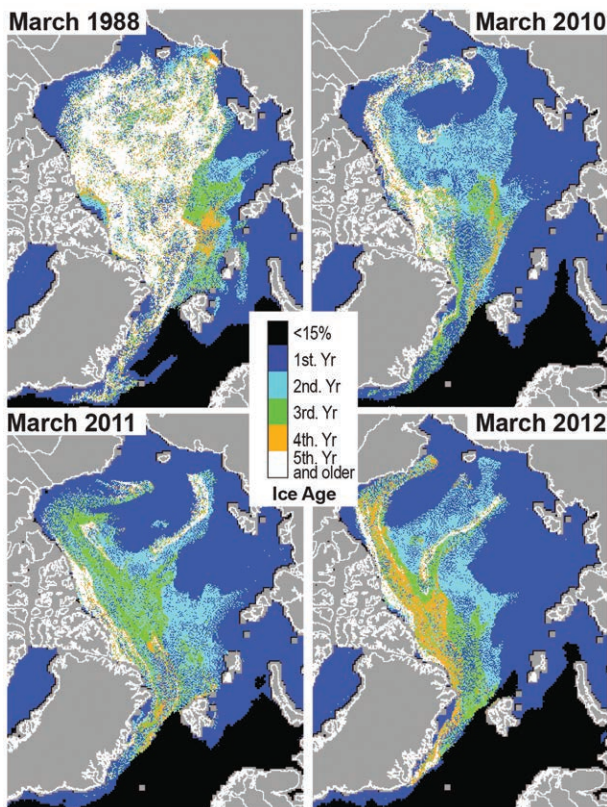


**FIG. 5.22. Sea ice age in March 1988, 2010, 2011, and 2012. Figure courtesy of M. Tschudi and J. Maslanik.**

and thus more resilient to changes in atmospheric and oceanic forcing than younger ice. The age of the ice is determined using satellite observations and drifting buoy records to track ice parcels over several years (Tschudi et al. 2010). This method has been used to provide a record of ice age since the early 1980s (Fig. 5.22).

The distribution of ice of different ages illustrates the extensive loss in recent years of the older ice types (Maslanik et al. 2011). Analysis of the time series of areal coverage by age category indicates the continued recent loss of the oldest ice types, which accelerated starting in 2005 (Maslanik et al. 2011). For the month of March, older ice (four years and older) has decreased from 26% of the ice cover in 1988 to 19% in 2005 and to 7% in 2012. This represents a loss of 1.71 million km<sup>2</sup> since 2005. In March 1988, 58% of the ice pack was composed of first-year ice (ice that has not survived a melt season). In March 2012, first-year ice dominated the pack (75%). Younger ice is typically thinner than older ice (e.g., Maslanik et al. 2007), so the current ice pack is thinner on average than it was in 1988. Note that from March 2011 to March 2012, much of the three-year-old ice north of the Canadian Archipelago survived the melt season, resulting in

an increase in four-year-old ice in March 2012 (5% compared to 2% in March 2011). This increase was directly associated with a reduction in the fraction of three-year-old ice, which decreased from 9% to 7%.

k. *Ocean temperature and salinity*—M.-L. Timmermans, I. Ashik, Y. Cao, I. Frolov, R. Ingvaldsen, T. Kikuchi, R. Krishfield, H. Loeng, S. Nishino, R. Pickart, B. Rabe, I. Semiletov, U. Schauer, P. Schlosser, N. Shakhova, W.M. Smethie, V. Sokolov, M. Steele, J. Su, J. Toole, W. Williams, R. Woodgate, J. Zhao, W. Zhong, and S. Zimmermann

1) UPPER OCEAN

Mean sea surface temperature (SST) anomalies in August 2012, relative to the August mean of 1982–2006, were more than 2°C higher in parts of the Beaufort, Laptev, and Kara Seas (Fig. 5.23). While most Arctic Ocean boundary regions displayed anomalously warm SST in 2012, a strong cold anomaly was evident in the Chukchi Sea. This was related to the sea ice extent pattern, which included the persistence of sea ice in this area even as the main ice pack retreated northward. In addition, a strong cyclonic storm during the first week of August (Sidebar 5.1) coincided with rapid degradation of this southern ice patch and anomalously cool SSTs for this time of year.

Relative to the 1970s Environmental Working Group (EWG) climatology (Timokhov and Tanis

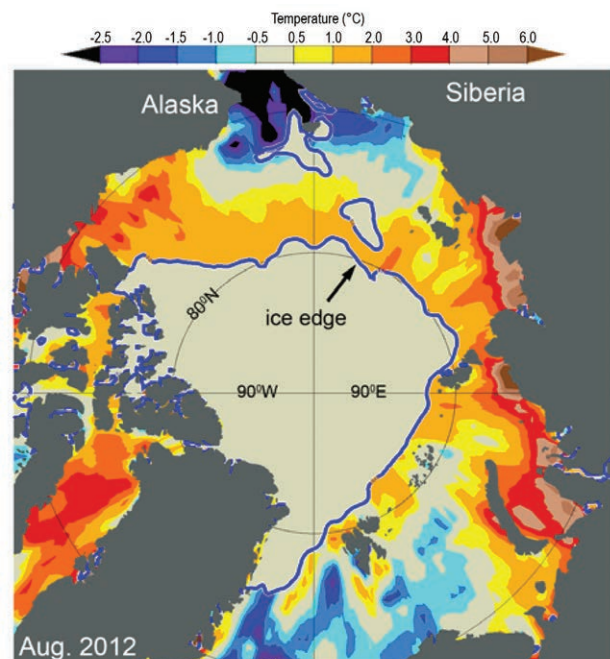


**FIG. 5.23. Sea-surface temperature (SST) anomalies (°C) in August 2012 relative to the August mean of 1982–2006. The anomalies are derived from satellite data according to Reynolds et al. (2007). The August 2012 mean ice edge (blue line) is also shown.**

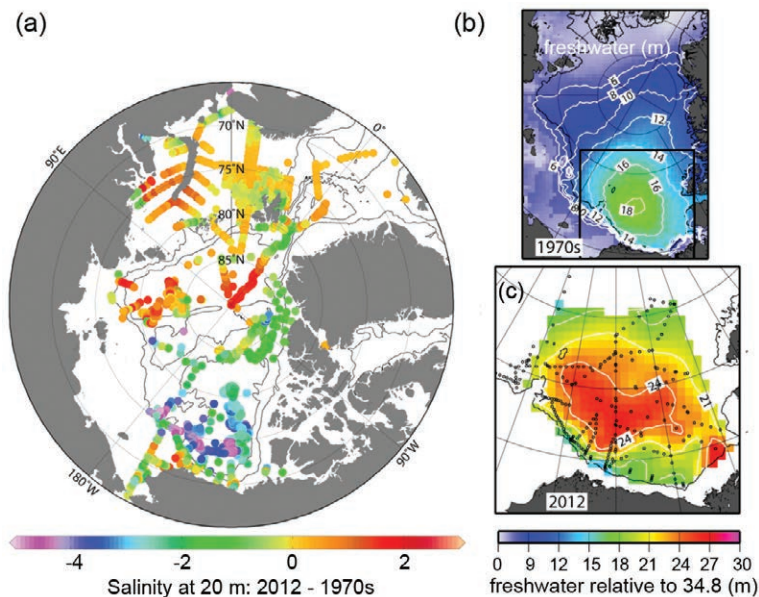


**FIG. 5.24. (a) Anomalies of salinity at 20-m depth in 2012 relative to 1970s climatology. Contour lines show the 500-m and 2500-m isobaths. (b, c) Freshwater content (m) calculated relative to a reference salinity of 34.8: (b) freshwater content in the Arctic Ocean based on 1970s climatology (Timokhov and Tanis 1997); (c) freshwater content in the Beaufort Gyre (the region enclosed by the black box in the top panel) based on hydrographic surveys (black dots depict station locations) in 2012.**

1997), the major upper-ocean salinity differences in 2012 (Fig. 5.24a) were saltier waters in the central Eurasian Basin and a fresher Canada Basin in general. The upper waters of the Barents and Kara Seas were predominantly anomalously salty relative to climatology, although the magnitude of the salinity difference was smaller than in the central Arctic Basin. In the region to the north of Greenland and Ellesmere Island, upper-ocean salinity in 2012 was only slightly less than the 1970s climatology, although small changes can be attributed in part to gaps in sampling.

The maximum freshwater content anomaly is centered in the Beaufort Gyre (BG), Canada Basin (Fig. 5.24c). The BG accumulated more than 5000 km<sup>3</sup> of freshwater during 2003–12, a gain of approximately 25% (update to Proshutinsky et al. 2009) relative to climatology of the 1970s (Fig. 5.24b). In 2012, the BG freshwater content was comparable to that in 2011, although 2012 saw a shift in the center of freshwater content to the northwest relative to 2011, consistent with the large-scale wind forcing (see Timmermans et al. 2012, figures 2.7, 2.11). The strong freshwater accumulation trend in the Beaufort Gyre has been linked to an increase in strength over the past decade of the large-scale anticyclonic wind forcing (e.g., Proshutinsky et al. 2009). Shifts in major freshwater

pathways also influence BG freshwater (Morison et al. 2012), while freshwater transported offshore during storms in the southern Beaufort Sea can also account for a significant fraction of the observed year-to-year variability in freshwater content of the BG (Pickart et al. 2013). The BG heat content in 2012 (see Timmermans et al. 2012, figure 2.11) also remained approximately comparable to 2011 conditions, with ~25% more heat on average in the summer compared to the 1970s.

## 2) ATLANTIC WATER LAYER

Warm water of North Atlantic origin, lying below the halocline at depths between about 200 m and 900 m (shallower in the vicinity of Fram Strait), is characterized by temperatures >0°C and salinities >34.5. In 2012 in the southern Barents Sea, Atlantic Water temperatures reached a maximum (since 1951) of up to 6°C, about 1.4°C higher than the long-term mean (1951–2010) and about 1.2°C

higher than in 2011 (Trofimov and Ingvaldsen 2012). In other regions, no significant changes were observed in 2012 in this layer compared to 2011 conditions. Relative to 1970s climatology, maximum Atlantic Water temperature anomalies are highest on the Eurasian side of the Lomonosov Ridge, with maximum anomalies 2°C in Fram Strait (see Proshutinsky et al. 2012, figure 5.22b). Warming is less pronounced in the Canada Basin, with Atlantic Water cooler now than in the 1970s in the region to the north of Ellesmere Island.

## 3) PACIFIC WATER LAYER

The Pacific Water layer in the Arctic Ocean originates from the Bering Strait inflow and resides in the Canada Basin at depths between about 50 m and 150 m. Data from ice-tethered profilers that sampled in the central Canada Basin during 2004–12 indicate Pacific Water warming in recent years that is broadly congruent with freshening. The maximum temperature of the Pacific Water layer increased by about 1.5°C over this time, with corresponding increases in heat content.

In 2011, the most recent year for which data are available, Pacific Water inflow through the Bering Strait was about 1.1 Sv (Woodgate et al. 2012), significantly

greater than the climatological value of about 0.8 Sv (Roach et al. 1995). The 2011 Bering Strait heat flux ( $\sim 5 \times 10^{20}$  J relative to  $-1.9^\circ\text{C}$ , the freezing point of Bering Strait waters) was comparable to the previous record high in 2007. The freshwater flux through the strait (relative to a salinity of 34.8) indicates the 2011 annual mean is  $3000 \text{ km}^3$ – $3500 \text{ km}^3$  (Woodgate et al. 2012), roughly 50% greater than 2001 and 2005 values. The interannual variability of the freshwater flux through the Bering Strait is larger than the interannual variability in the other major freshwater sources to the Arctic, i.e., rivers and net precipitation.

#### *l. Ocean acidification*—J. T. Mathis, C. Hauri, and J. N. Cross

It has been widely shown that the uptake of anthropogenic  $\text{CO}_2$  by the oceans (e.g., Sabine et al. 2004, 2007) has a significant effect on marine biogeochemistry by reducing seawater pH (e.g., Feely et al. 2009; Caldiera and Wickett 2003) and the saturation states ( $\Omega$ ) of important calcium carbonate ( $\text{CaCO}_3$ ) minerals (Feely et al. 2004; Orr et al. 2005; Caldiera and Wickett 2005) through a process termed “ocean acidification”.

However, the uptake of anthropogenic  $\text{CO}_2$  is not the only process that can reduce  $\Omega$ . There are several

## **SIDEBAR 5.2: TOWARD AN INTERNATIONAL NETWORK OF ARCTIC OBSERVING SYSTEMS—C. M. LEE, J. ZHAO, AND M. JAKOBSSON**

Arctic environmental change, exemplified in this chapter, motivates research and observations to quantify secular trends, understand the driving mechanisms and feedbacks, and improve predictability of both Arctic change and its impact on global climate. Local needs also drive observing activities, as Arctic residents, government, and industry require information over a range of timescales to inform their response to the changing environment. An integrated international network of Arctic observing systems (AOS), spanning a broad range of spatial and temporal scales and providing the multiyear persistence required to resolve secular trends, is needed to meet these varied demands.

The pan-Arctic scope and decadal outlook define a broad, inherently international, network of observing systems. An AOS must provide data to meet needs that fall under three overlapping domains, loosely termed policy, strategy, and tactics. Policy ties closely to governance, demanding an understanding of environmental change to inform long-term planning (decades), disaster mitigation (prevention and preparedness, response, recovery), regulation, and environmental protection. Value is placed on long records compiled from sustained, consistent measurements distributed around the Arctic.

At the strategy level, government, industry, and local communities require data to carry out medium-term planning (seasons to years) of expensive or hazardous activities. Examples include assessing feasibility of shipping across the Arctic Ocean and engineering to support resource extraction. Data needs can be more geographically localized than those of the climate network, and strategy-level observing systems may exist at both national and international scales.

Tactical needs involve the supply of data products to answer short-term (hours to weeks) requirements, such as guiding safe, efficient travel and informing hunting and fishing activity. This demands real-time delivery and may involve highly localized systems driven at the community level.

This conceptual framework guides the design and development of a broad range of Arctic observing systems and their coordination into a broader, sustainable network. While challenging in scope and longevity, a nested, network-of-systems structure allows individual components to be planned and executed at tractable scales. This approach also facilitates implementation of flexible systems capable of evolving in response to environmental challenges and shifting priorities.

Significant effort has been invested in planning for an AOS. For example, the Study of Environmental Arctic Change (SEARCH 2005), the U.S. Polar Research Board (2006), and Interagency Arctic Research Policy Committee (IARPC 2007) discuss potential U.S. contributions to a pan-Arctic observing network. The Arctic Ocean Science Board (AOSB 2005) outlined an international plan for integrated Arctic observing during the IPY 2007–2008. More recently, the Arctic Regional Ocean Observing System provides an example of international integration, with institutions from nine European countries integrating diverse observational and modeling efforts to provide operational monitoring and forecast capability (<http://www.arctic-roos.org>). The International Study of Arctic Change (ISAC 2009) facilitates cooperative, international efforts to understand the future state of the Arctic, while the Sustained Arctic Observing Network (SAON; <http://www.arcticobserving.org>) seeks avenues for international collaboration, governance, and support of observing activities. A biennial Arctic Observing Summit (a contribution to SAON), first held in May 2013, serves as a forum for planning and coordinating network activities, and for identifying approaches for overcoming pan-national challenges.

In broad terms, an AOS would consist of distributed observing networks, flagship observing sites, and hybrid systems. Distributed networks, such as the International Arctic Buoy Programme, collect key measurements at a large number of sites, typically with broad, pan-Arctic or regional coverage.

other drivers in the western Arctic Ocean, such as sea ice melt (Yamamoto-Kawai et al. 2009), respiration of organic matter (Bates and Mathis 2009), upwelling (Mathis et al. 2012), and riverine inputs (Mathis et al. 2011), that can exacerbate ocean acidification at different temporal and spatial scales. These processes, combined with the fact that the Arctic Ocean is already pre-conditioned to have relatively low  $\Omega$  compared to the global ocean due to lower temperatures and unique physical and biogeochemical processes (Fabry et al. 2009), make the region highly vulnerable to further reductions in seawater pH, with

In contrast, flagship observatories focus resources on critical locations to provide extensive suites of measurements, albeit with limited spatial extent. Examples include the Zackenberg, Greenland, ecosystem research and observing station, and the arrays of heavily instrumented moorings at Bering, Fram, and Davis straits that quantify exchanges between the Arctic and subarctic oceans at critical gateways. The International Arctic Systems for Observing the Atmosphere (IASOA), a network of ten flagship atmospheric observatories distributed around the Arctic Ocean rim, is an example of a hybrid system. These systems share a common characteristic: all were designed to deliver regular, climate-quality measurements sustained over time spans of years to decades. The AOS also requires an improved geospatial framework (e.g., coastlines, seafloor bathymetry, and land topography) to support modeling, interpretation, and understanding. Focused, intensive, short-term studies also play a significant role, advancing understanding of key processes at scales that long-term measurements cannot resolve.

Cooperation is essential to achieve a sustained, integrated AOS. At the local level, this should include community-based monitoring and indigenous observations. At the national level, agencies responsible for basic research and operational observing must cooperate to develop models for supporting long-term, integrated measurement efforts capable of meeting the immediate, tactical needs of Arctic stakeholders while also producing the broadly distributed, long time series needed to investigate climate change and its impacts. International coordination will be required to optimize these national plans for fit within the broader scope of the pan-Arctic network, to facilitate shared logistics and ensure the open sharing of data. International collaboration and coordination will also play a critical role in identifying sustainable funding models, optimizing activities across diverse observing systems and securing pan-Arctic access for the basic scientific research performed by the network (Calder et al. 2009).

unknown, but likely detrimental, consequences for certain marine organisms.

Unfortunately, there are no long-term observations of carbonate chemistry in the Arctic Ocean, as these properties were not measured until the early 2000s. Over the past several years, the number of observations has increased substantially (e.g., Mathis et al. 2012; Cai et al. 2010; Bates et al. 2009), although a number of questions remain regarding spatial variability and the seasonally varying controls on carbonate mineral saturation states.

In October 2012, an unprecedented survey was conducted in the Beaufort and Chukchi Seas from the USCGC *Healy*, with thousands of observations made of the carbonate system across the broadest area to date (Fig. 5.25). All four carbonate parameters (dissolved inorganic carbon, total alkalinity, pH, and the partial pressure of  $\text{CO}_2$ ) were directly measured at the surface, and three (dissolved inorganic carbon, total alkalinity, and pH) were directly measured in the water column.

The broad extent of these observations shows that there is a contrast in aragonite saturation states between the Chukchi Sea region and areas of the Beaufort Sea to the east. These spatial differences reveal the varying degree of impacts that primary production, ice melt, and river water can have on carbonate mineral concentrations and ocean acidification in the region. High rates of primary production over the Chukchi shelf consume dissolved inorganic carbon at the surface and cause a significant increase in pH and carbonate mineral saturation states (i.e., anti-ocean acidification) during spring and summer; these effects can be seen throughout the open-water season. Rates of primary production are much lower in the Beaufort Sea due to nutrient limitations; accordingly, the saturation states near the surface are lower. In the Canada Basin, where ice melt is most prevalent and rates of primary production are minimal, the surface waters are near undersaturation ( $\Omega < 1$ ) with respect to aragonite. Low  $\Omega$  waters were also observed north of the Bering Strait, where the Alaska Coastal Current (ACC) brings low salinity, carbonate-poor waters northward from the Bering Sea.

Water column measurements in 2012 confirmed previous observations (Bates and Mathis 2009) that subsurface waters over the Chukchi shelf, particularly in the region of Bar-

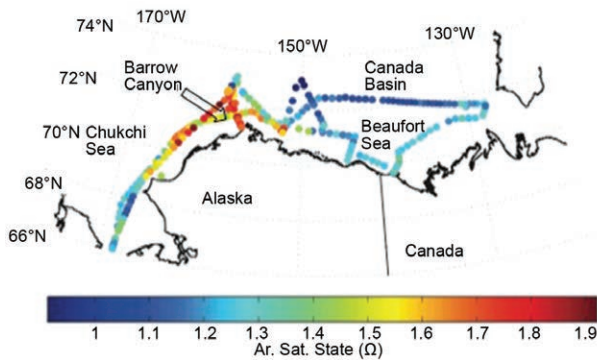


**FIG. 5.25. Aragonite saturation states ( $\Omega$ ) in October 2012 at the surface of the Beaufort and Chukchi Seas. When  $\Omega = 1$ , seawater is exactly in equilibrium or saturation with respect to aragonite. When  $\Omega > 1$ , the seawater is supersaturated with respect to aragonite and it precipitates. When  $\Omega < 1$ , the seawater is undersaturated with respect to aragonite and it dissolves.**

row Canyon (Fig. 5.25), can become undersaturated due to the accumulation of remineralized dissolved inorganic carbon. The waters on the western side of the canyon were highly undersaturated with respect to aragonite, which is consistent with the understanding of patterns of primary production and export of organic matter in the region (Mathis et al. 2007; Grebmeier et al. 2012). Figure 5.26 shows that the eastern part of the transect across Barrow Canyon was dominated by ACC water that was warmer, fresher and had lower total alkalinity. This riverine water is also low in inorganic nutrients and therefore limits primary production at the surface. However, observations on the western side of this transect were more indicative of central Chukchi Sea waters that are replete with nutrients and support high rates of primary production. The respiration signal is present near the bottom, with high dissolved inorganic carbon concentrations on the western side of the canyon.

The long-term drivers of ocean acidification in the western Arctic will continue to be the loss of seasonal sea ice, which will allow greater interaction with the anticipated higher atmospheric  $\text{CO}_2$  concentrations and will directly reduce carbonate mineral concentrations through dilution at the surface.

In addition, the loss of ice will allow for increases in the frequency, intensity, and duration of wind-driven upwelling events that have been shown to bring waters that are undersaturated in carbonate minerals to the surface (Mathis et al. 2012). The changes in the carbonate system caused by these drivers will be reinforced by natural respiration processes related to the production and export of organic matter, both of which will likely increase in a warmer, sea ice-depleted Arctic (Arrigo and van Dijken 2011). It will be critical to understand the timing, duration, and spatial extent of undersaturation events both at the surface and in bottom waters, particularly as they relate to species distribution and sensitive life stages of calcifying organisms.

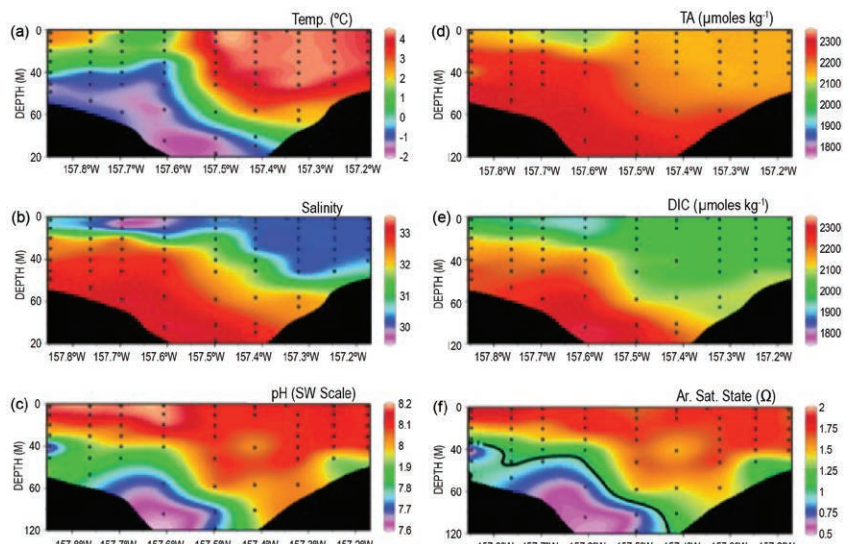


**FIG. 5.26. Cross-sections of (a) temperature, (b) salinity and several carbonate parameters [(c) pH, (d) total alkalinity (TA), (e) dissolved inorganic carbon (DIC), and (f) aragonite saturation state ( $\Omega$ )] in Oct 2012 midway along Barrow Canyon (Fig. 5.25). The plots are scaled such that the middle area is the deepest part of the canyon viewed from the south, i.e., looking northward towards the mouth of the canyon and the Arctic Ocean.**